Catalysis Science & Technology

ROYAL SOCIETY OF CHEMISTRY

PERSPECTIVE

Check for updates

Cite this: *Catal. Sci. Technol.*, 2023, **13**, 2274

Sm_2O_3 and Sm_2O_3-based nanostructures for photocatalysis, sensors, CO conversion, and biological applications

Mohammad Mansoob Khan * and Shaidatul Najihah Matussin

Received 18th November 2022,
Accepted 3rd March 2023

DOI: 10.1039/d2cy01976k

rsc.li/catalysis

Metal oxide nanoparticles have gained popularity owing to their unique properties. Recently, metal oxides, particularly rare-earth metal oxides, have been explored and used in several areas. Samarium oxide (Sm_2O_3) amongst other rare-metal oxides is no exception. It has a band gap of about 4.3 eV and suitable dielectric properties. Different morphologies and structure-based Sm_2O_3 and Sm_2O_3-based nanostructures have been fabricated using different synthesis methods such as precipitation, hydrothermal, combustion, green synthesis, *etc.* Additionally, various applications of Sm_2O_3 and Sm_2O_3-based nanostructures have also been investigated. The reported properties impact the response towards the applications such as photocatalysis, sensors, CO conversion, and biological applications. Therefore, in this perspective, different synthesis methods, characteristics, mechanisms, and varieties of applications of Sm_2O_3 and Sm_2O_3-based nanostructures have been investigated and discussed.

1.0. Introduction

Nanoparticles (NPs) are ultrasmall particles (1–100 nm) in which significant numbers of atoms are located in the interfacial structure in a disordered manner, resulting in novel physical and chemical properties.[1] Metal oxide NPs,

Chemical Sciences, Faculty of Science, Universiti Brunei Darussalam, Jalan Tungku Link, Gadong, BE 1410, Brunei Darussalam. E-mail: mmansoobkhan@yahoo.com, mansoob.khan@ubd.edu.bn

Mohammad Mansoob Khan

Mohammad Mansoob Khan earned his MSc and Ph.D. degrees from Aligarh Muslim University, Aligarh, India. After his Ph.D., he has taught in different countries (India, Ethiopia, Oman, and South Korea) for about twenty years. Currently, he is working as a Professor at Chemical Sciences, Faculty of Science, Universiti Brunei Darussalam, Brunei Darussalam. His current research interests include green synthesis of metal nanoparticles, metal oxide nanoparticles, band gap engineering of metal oxides, metal oxide-based nanocomposites, graphene-based nanocomposites, and chalcogenides through novel and simple methods. Synthesized nanomaterials are used for various energy, environment, and biologically related applications such as visible light harvesting, visible light-induced photocatalysis, optoelectronic devices, photoelectrodes, H_2 production, and antibacterial, antioxidant, and wound healing applications.

Shaidatul Najihah Matussin

Shaidatul Najihah Matussin is currently pursuing PhD under the supervision of Prof. Mohammad Mansoob Khan, at the Department of Chemical Sciences, Faculty of Science, Universiti Brunei Darussalam. She obtained her BSc degree from the same university. Her current research interests include green synthesis of metal oxide nanoparticles and nanocomposites for potential applications such as photocatalysis and antioxidant activities.

particularly transition metals, have wide applications due to their rich valence states, vast surface areas, and varying electronic structures which include catalysis, electronics, and optical and magnetic sensors. Depending on the overall shape, these materials can be 0D, 1D, 2D, or 3D. The size of nanoparticles can be crucial as it can influence the physicochemical properties of the NPs.[2,3] NPs are categorized into different classes and one of them is semiconductor NPs. Semiconductor materials possess properties between metals and nonmetals and therefore various applications have been found. Semiconductor NPs have wide band gaps in which studies showed significant modification in their properties with band gap tuning.[4] Metal oxide NPs have been produced by synthesis methods such as sol–gel,[5–8] pyrolysis,[9–11] hydrolysis,[12–14] and gas-phase condensation techniques.[15]

Amongst metal oxides, rare earth oxides (RE_2O_3) have attracted considerable attention due to their optical, electronic, and chemical properties resulting from their 4f electrons, and rare earth oxides have been widely used in the fields of luminescence devices, optical transmission, biochemical probes, medical diagnostics, and so forth.[16,17] They are the most stable rare earth compounds, in which the rare earth ions hold typically a trivalent state.[16] It is known that RE_2O_3 nanostructures exhibit improved catalytic and luminescence properties. Therefore, considerable efforts have been devoted to producing RE_2O_3 nanocrystals.[18] All the rare-earth elements form a sesquioxide of RE_2O_3 and have five different crystallographic phases. At temperatures lower than about 2273 K, three types of phases: hexagonal $P32/m$, monoclinic $C2/m$, and cubic $Ia3$ are usually observed, and for temperatures higher than 2273 K, the hexagonal and cubic phases are formed. When increasing the temperature, the order of phase transition is from cubic $Ia3$ to monoclinic $C2/m$ and to hexagonal $P32/m$, even though not every oxide will show all phases. This common transition is characteristic of the intermediate elements of the group.[19] Most crystallographic phase diagrams in the literature are for bulk materials, and only a few present or discuss the phase diagrams of their nanostructure materials. Therefore, the differences between bulk and nanomaterials are important to comprehend, since they affect the final product properties.[19]

Sm_2O_3 is a typical lanthanide oxide that has attracted considerable interest in photocatalysis and electrocatalysis in which cubic Sm_2O_3 crystallizes in the bixbyite type which may be described as a 2 × 2 × 2 superstructure of the fluorite type with one quarter of the anion positions being vacant (Fig. 1).[20] This material has been extensively studied due to its potential applications in various fields. Sm_2O_3 is a p-type semiconductor which has a tendency to exchange lattice oxygen easily with air. This can be useful in maintaining stoichiometry of the oxides. Sm_2O_3 is considered as the most promising candidate for future gate dielectrics in Si-MOS based devices.[21] Sm_2O_3 has the second highest k-value among the rare-earth oxides which makes it an alternative candidate for high-k materials. Moreover, its band gap and conduction band offset have fulfilled the basic requirements of a high-k dielectric. The most important feature is the hygroscopic nature of Sm_2O_3 as it has a smaller ionic radius and it is less electropositive.[22,23]

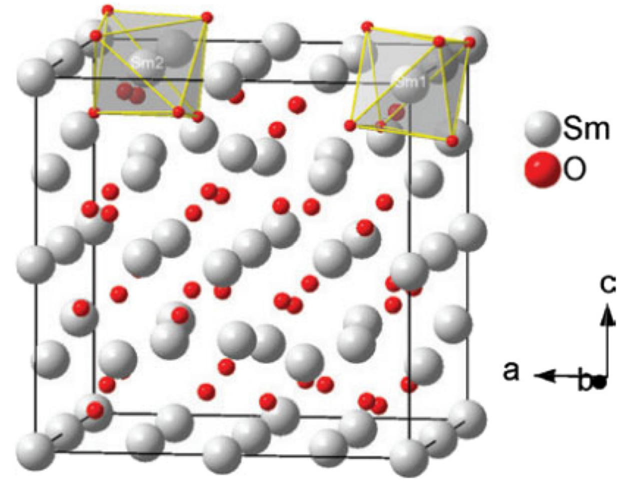

Fig. 1 Crystal structure of cubic Sm_2O_3 in the bixbyite type at T = 298 K and coordination polyhedra of the Sm1 (right) and Sm2 (left) atoms.[20] This figure has been adapted from ref. 20 with permission from De Gruyter, copyright 2023.[20]

Shape-controlled Sm_2O_3 nanocrystals are promising building blocks for the bottom-up assembly of novel nanostructures with high potential applications in various fields, such as in solar cells,[24] nanoelectronics,[25] gas sensors,[26] and biochemical sensors.[27] Furthermore, Sm_2O_3 could act as an effective catalyst for the oxidative coupling of methane with high activity, selectivity, and durability.[28] Sm_2O_3 and Sm_2O_3-based materials have been prepared using various synthesis methods such as precipitation, sol–gel, hydrothermal, solid state and green synthesis.

To the best of the authors' knowledge, in the past few years, no review on the development and in-depth discussion on Sm_2O_3 and Sm_2O_3-based materials have been produced. Therefore, in this review, the fabrication of Sm_2O_3, doped-Sm_2O_3, and Sm_2O_3-based materials using different synthesis routes and method parameters has been discussed. The effects of different synthesis methods on the applications have also been explained. The applications of Sm_2O_3 and Sm_2O_3-based materials as well as their mechanisms have been reported in this review.

2.0. Synthesis of Sm_2O_3

Sm_2O_3 has been synthesized through various synthesis methods (Fig. 2). Mohammadinasab *et al.* synthesized spherical Sm_2O_3 particles with a crystallite size of 50 nm using the thermal decomposition synthesis method.[29] Thermal decomposition is considered as a method to synthesize stable monodispersed NPs. $Sm(NO_3)_3·6H_2O$ was used and dissolved in polyethylene glycol. The reaction was carried out at 150 °C and the product was dried at 100 °C. Ubale *et al.* prepared the cubic phase of Sm_2O_3 NPs using a

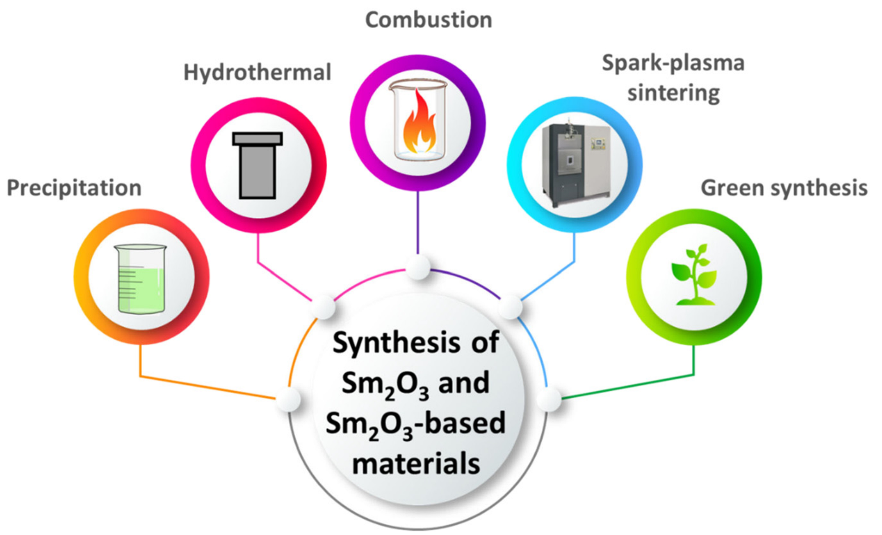

Fig. 2 Various synthesis methods of Sm_2O_3 and Sm_2O_3-based materials.

one pot hydrothermal method.[30] $SmCl_3·7H_2O$ was mixed with urea and tartaric acid and heated at 121 °C for 3 h. Groundnut-like particles were obtained with a crystallite size of 8.3 nm. Sm_2O_3 microparticles of 1–10 μm were obtained through a hydrothermal method as stated by Jamnani *et al.*[31] Citric acid was used as the solvent and $Sm(NO_3)_3·6H_2O$ as the precursor. The reaction was heated at 180 °C for two different durations: 24 h and 36 h. The drying was done in an oven at 100 °C for 2 h and the product was subjected to calcination at 800 °C for 2 h. The Sm_2O_3 microparticles were observed to be microspheres. Sm_2O_3 microspheres were tested for volatile organic compound (VOC) monitoring. Other Sm_2O_3 microparticles were prepared using the same precursor according to Michel *et al.*[32] A co-precipitation method was utilized. The precursor was stirred in formic acid at room temperature for 20 h and dried at 140 °C. The product was then calcined at 300 to 600 °C and particles between 1 and 6 μm were obtained. The particles were spherical and they were found out to be suitable for CO and CO_2 sensing. Sm_2O_3 nanorods were utilized for CO gas sensing in Jamnani's work.[33] $Sm(NO_3)_3·6H_2O$, ammonia and CTAB were mixed together in an autoclave vessel and heated at 120 °C for 3 h through a hydrothermal reaction. The Sm_2O_3 nanorods were calcined at 600 °C for an hour before they were used as a CO gas sensor. The nanorods were 400 nm in length and 80 nm in diameter. Kang *et al.* reported on the formation of $Sm(OH)_3$ nanoroll sticks in which the product was calcined at 450 °C to form Sm_2O_3.[34] Interestingly, the morphology was retained after treatment with high temperature. The amount of ammonia was stated to play a major role in determining the morphology.

Sm_2O_3 NPs were obtained *via* a green synthesis using *Casllistemon viminalis* extract as stated by Sone *et al.*[35] Sm(III) acetyl acetonate was used and the reaction solution was heated at 80 °C for 1 h and calcined at 500 °C. Small quasi-spherical particles of about 21.9 nm were obtained. Tamboli *et al.* used a precipitation method with $SmCl_2·6H_2O$ as the precursor and urea.[36] The reaction was carried out at 120 °C and the product was dried at 60 °C for 12 h. This method produced a sweet corn-like structure with a diameter of 265 nm and a length of up to 1443 nm. The obtained Sm_2O_3 was applied for 2-azidoalcohol synthesis. Hierarchical clew-like Sm_2O_3 microspheres were obtained by Yin *et al.* through a hydrothermal reaction.[37] $Sm(NO_3)_3·6H_2O$ and urea were mixed together in the reaction and heated at 180 °C for 24 h and the mixture was subsequently dried at 60 °C for 3 h. The product was calcined at 600 °C for 1 h producing clew-like Sm_2O_3 particles of about 3 μm. Yin *et al.* synthesized Sm_2O_3 particles *via* a hydrothermal synthesis method.[38] Two different solvents were used in the reaction, *i.e.* NaOH and HCl mixed with the $SmCl_3·6H_2O$ precursor. The synthesis reaction was carried out at 200 °C for 48 h and the product was calcined at 800 °C for 1 h. Two different morphologies were produced. Sm_2O_3 nanorods were obtained when NaOH was used as the solvent while a ribbon-like structure was obtained when HCl was used as the solvent. Sm_2O_3 nanorods were found to be 2 micrometers long and 100 nm wide, whereas Sm_2O_3 nanoribbons were 200 nm (Fig. 3).

Sm_2O_3 NPs were obtained through an *Andrographis paniculata* leaf extract-mediated green synthesis as stated by Muthulakshmi *et al.*[39] $SmCl_3·6H_2O$ was mixed with the leaf extract and stirred at room temperature. The product was annealed at 600 °C for 6 h. The obtained particles were cubic-like with an average size of 30 to 50 nm. The antibacterial, antioxidant and bovine serum albumin denaturation inhibition properties of Sm_2O_3 NPs were investigated. A Sm_2O_3 porous foam-like morphology was obtained *via* a solvo-combustion method according to Ruiz-Gómez *et al.*[40] Samarium (III) acetate hydrate was mixed in acetylacetone, ethanol and nitric acid which was refluxed at 70 °C. The solvents were evaporated at 180 °C. The final product was calcined at elevated temperature, *i.e.* 400–800

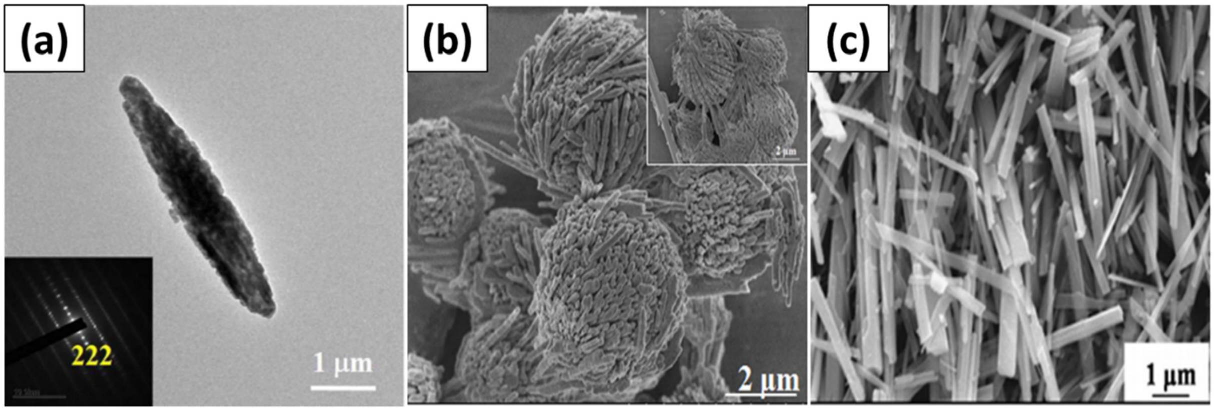

Fig. 3 SEM images of corn-like, clew-like and ribbon-like Sm_2O_3 NPs.[36–38] Figure (a) has been adapted from ref. 36 with permission from *Colloids and Surfaces A*, copyright 2023, figure (b) has been adapted from ref. 37 with permission from *Materials Letters*, copyright 2023, and figure (c) has been adapted from ref. 38 with permission from *Materials Science in Semiconductor Processing*, copyright 2023.[36–38]

°C. Mesoporous Sm_2O_3 was synthesized by Yan *et al.* through a hydrothermal reaction.[41] $Sm(NO_3)_3·6H_2O$ was used in the synthesis and a mixture of glucose, acrylic acid and ammonia solution was used as the solvent. The synthesis reaction was carried out at 180 °C for 72 h. The final product was calcined at 600 °C under an argon atmosphere and the calcination was continued at 500 °C for 4 h under an air atmosphere. Nanosheet-like Sm_2O_3 was obtained with an average size of 3–6 μm and a thickness of 5 nm.

Yu *et al.* synthesized Sm_2O_3 using samarium acetate and a mixture of oleylamine and decanoic acid *via* a thermal decomposition method.[42] The reaction was heated at 90 °C in a vacuum to remove solvents and it was finally heated at 240 °C and aged for 6 h. Ultrasmall particles of Sm_2O_3 nanowires and nanoplates were obtained which showed an average size of 1.1 nm and 2.2 nm in length. A hydrothermal method was used to synthesize Sm_2O_3 thin films in Huang's work.[43] $SmCl_3·6H_2O$ and ammonia solution were used in the reaction. A low temperature of 45 °C was used for mixing and the reaction was heated at 180 °C for 2 h. The crystallite size of the synthesized Sm_2O_3 thin film was found to be 1–12 nm. Photochemical synthesis of Sm_2O_3 was conducted by Hodgson *et al.*[44] $Sm(NO_3)_3·6H_2O$, DMF and DMSO were used in the synthesis. Spherical Sm_2O_3 with an average size of 417 nm was obtained.

Fu *et al.* prepared Sm_2O_3 with three different morphologies namely, nanobelts, nanorods and nanotubes.[45] A hydrothermal reaction was utilized using ammonia solution as the solvent and $Sm(NO_3)_3·6H_2O$. The synthesis was done at 110 °C for 12 h and the product was calcined at 800 °C for 1 h producing Sm_2O_3 nanobelts, nanorods and nanotubes. Sm_2O_3 nanobelts were 200 nm in width and 1–2 μm in length, while the nanorods were 20 nm wide and 400 nm long. Finally, the nanotubes were 50 to 100 nm. Jiang *et al.* synthesized Sm_2O_3 NPs by a hydrothermal reaction using $Sm(NO_3)_3·6H_2O$ and 4-nitrobenzoic acid which was heated at 150 °C for 3 h.[46] Subsequently, the product was calcined at 600 °C for 2 h. The synthesized Sm_2O_3 NPs were found to be 40 nm and they were observed to be a highly sensitive and selective isobutyraldehyde sensor. Foam-like Sm_2O_3 NPs have been prepared by Mora-Ramírez *et al.* through chemical bath deposition.[47] An average grain size between 22.10 and 28.20 nm was obtained which showed optical absorption bands located at ~277 nm and ~408 nm in the UV-vis region. Sm_2O_3 nanoplatelets have been synthesized using the electrodeposition technique.[48] $SmCl_3·6H_2O$ was mixed with KCl at 90 °C by applying a potential of −0.80 V *vs.* SCE producing a complete surface coverage of high porosity Sm_2O_3 nanoplatelets. Table 1 shows the various synthesis methods of pure Sm_2O_3.

3.0. Synthesis of doped-Sm_2O_3 particles

Co-doped Sm_2O_3 was synthesized using a co-precipitation technique as reported by Mandal *et al.*[50] In this case, commercially available Sm_2O_3 and $CoCl_2·6H_2O$ were used and stirred together with HCl and NaOH. The reaction was carried out at room temperature with subsequent calcination at 700 °C for 6 h. Spherical Co-doped Sm_2O_3 with a particle size of 13 to 50 nm was obtained. Aswathy *et al.* synthesized Co-doped Sm_2O_3 through a combustion method.[51] $Sm(NO_3)_3·6H_2O$ and $Co(NO_3)_2·6H_2O$ were mixed in glycine solution and it was heated at 700 °C for 2 h and sintered at 900 °C for 10 h. The synthesized Co-doped Sm_2O_3 particles were porous which showed a particle size between 75 and 90 nm. The synthesis of Ni-doped Sm_2O_3 was reported by Zhang *et al.*[52] A precipitation method was utilized using $Ni(NO_3)_2·6H_2O$ and $Sm(NO_3)_3·6H_2O$ as the precursors and EDTA and NaOH as the additives. The synthesis was carried out at room temperature and elevated to 70 °C as NaOH was added. The product was dried at 120 °C and calcined at 800 °C for 6 h obtaining a crystallite size between 107 and 129 nm. Ru-doped Sm_2O_3 NRs were synthesized by Zhang *et al.* using a precipitation method. The obtained sample was reduced in H_2/Ar stream at 500 °C for 2 h.[53] Ru-doped Sm_2O_3

Table 1 Synthesis of pure Sm_2O_3 using various synthesis methods

No.	Synthesis method	Precursors	Particle size	Morphology	Applications	Ref.
1	Thermal decomposition	$Sm(NO_3)_3 \cdot 6H_2O$	—	Spherical	—	29
2	One-pot hydrothermal	$SmCl_3 \cdot 6H_2O$	—	Groundnut-like	—	30
3	Hydrothermal	$Sm(NO_3)_3 \cdot 6H_2O$	1–10 μm	Microspheres	VOC monitoring	31
4	Co-precipitation	$Sm(NO_3)_3 \cdot 6H_2O$	1–6 μm	Spheres	Gas sensing	32
5	Hydrothermal	$Sm(NO_3)_3 \cdot 6H_2O$	400 nm (length) and 80 nm (diameter)	Nanorods	—	33
6	Green synthesis	Sm(III) acetyl acetonate	16–27 nm	Quasi spherical	—	35
7	Precipitation	$SmCl_3 \cdot 6H_2O$	265 nm (diameter) and 1443 nm (length)	Sweet-corn like	2-Azidoalcohol synthesis	36
8	Hydrothermal–calcination	$Sm(NO_3)_3 \cdot 6H_2O$	3 μm	Clew-like	—	37
9	Hydrothermal–calcination	$SmCl_3 \cdot 6H_2O$	Nanorods – 2 μm (length) and 100 nm (diameter) Ribbon-like – 200 nm	Nanorods and ribbon-like	—	38
10	Green synthesis	$SmCl_3 \cdot 6H_2O$	Cubic	30–50 nm	Antibacterial, antioxidant and inhibition of bovine serum denaturation	39
11	Solvo-combustion	Samarium(III) acetate hydrate	—	Foam-like	—	49
12	Hydrothermal	$Sm(NO_3)_3 \cdot 6H_2O$	3–6 μm and 5 nm (thickness)	Nanosheets	Hydrogen peroxide sensor	41
13	Thermal decomposition	Samarium(III) acetate hydrate	1.1 nm (width) and 2.2 nm (length)	Nanowires and nanoplates	—	42
14	Hydrothermal	$SmCl_3 \cdot 6H_2O$	—	Thin films	—	43 44
15	Photochemical	$Sm(NO_3)_3 \cdot 6H_2O$	417 nm	Spherical	—	45
16	Hydrothermal	$Sm(NO_3)_3 \cdot 6H_2O$	Nanobelts – 200 nm (width) and 1–2 μm (length) Nanorods – 20 nm (width) and 400 nm (length) Nanotubes – 5 to 100 nm	Nanobelts, nanorods and nanotubes	—	
17	Hydrothermal	$Sm(NO_3)_3 \cdot 6H_2O$	40 nm	—	Isobutyraldehyde sensor	46
18	Green chemical bath deposition	$Sm(NO_3)_3 \cdot 6H_2O$	22.10–28.20 nm	Foam-like	—	47
19	Electrodeposition	$SmCl_3 \cdot 6H_2O$	—	Nanoplatelets	Biosensor	48

NRs were 100–600 nm in length and 30–60 nm in width. In this study, the metal interaction with Sm_2O_3 was found to enhance NH_3 decomposition.

3.1. Synthesis of semiconductors using Sm_2O_3 as a dopant and a metal surface decoration

On the other hand, Sm_2O_3 has also been reported to have been used as a dopant. For example, Sm_2O_3-doped SnO_2 NPs were produced in a study conducted by Feyzabad *et al.*[54] A combustion method was used to produce Sm_2O_3-doped SnO_2 using $SnCl_4$ and $Sm(NO_3)_3 \cdot 6H_2O$ as the precursors, $C_6H_{14}O_6$ as the fuel and NH_4NO_3 as the combustion aid. The whole reaction was heated at 100 °C for 15 min and exposed in a microwave oven for another 15 min. The final product was calcined at 400 °C for 3 h. The particles were agglomerated showing a particle size between 100 and 300 nm. The gas sensing ability of synthesized Sm_2O_3-doped SnO_2 in the presence of VOCs was investigated. In another study, Sm_2O_3-doped SnO_2 NPs were also fabricated using the same synthesis method as stated by Habibzadeh *et al.*[55] However, commercially available Sm_2O_3 was used in the synthesis with $SnCl_4$, nitric acid, sorbitol and NH_4NO_3. Similarly, agglomerated particles were observed showing a particle size between 50 and 200 nm. The gas sensing properties of the synthesized Sm_2O_3-doped SnO_2 NPs were investigated as well. Sm_2O_3-doped SnO_2 thin films were fabricated through a precipitation technique in a study conducted by Shaikh *et al.*[56] $SnCl_4 \cdot 5H_2O$, $Sm(NO_3)_3 \cdot 6H_2O$ and NH_4OH were used in the synthesis which was carried out at room temperature only. The final product was calcined at 450 °C for 2 h. Ultrasmall irregular shaped Sm_2O_3-doped SnO_2 about 5–8 nm was obtained. The performance of acetone sensing using the synthesized material was enhanced.

Sm_2O_3-doped CeO_2 NPs were also fabricated and used as a photocatalyst to degrade acid orange 7 as reported by Mandal *et al.*[57] A crystallite size of about 7 to 22 nm was obtained *via* a surfactant assisted microwave reaction. Yao *et al.* synthesized CoO–Sm_2O_3 co-doped CeO_2 *via* a co-precipitation method which was carried out at room temperature.[58] The product was dried at 60 °C, calcined at 600 °C for 4 h and sintered at 1200 to 1400 °C for 4 h producing porous particles between 0.5 and 3 μm. Ibrahim *et al.* prepared Sm_2O_3-doped ZnO as a nitroaniline chemical sensor using a hydrothermal method.[59] H_2O and NH_4OH were used to mix with Zn acetate and $Sm(NO_3)_3 \cdot 6H_2O$ in an autoclave which was heated at 155 °C for 7 h. The product was dried at 70 °C for 4 h producing needle-shaped particles with 0.5 μm in diameter and 9–10 μm in length. Table 2 summarizes the methods to prepare doped Sm_2O_3 and Sm_2O_3-doped metal oxide NPs.

4.0. Synthesis of Sm_2O_3-based materials

Samarium oxide supported cobalt catalysts were synthesized through a wet impregnation method as reported by Ayodele *et al.*[60] The synthesis was carried out at room temperature in which the product was calcined after that at 600 °C for 6 h. Cubic phase Sm_2O_3 supported Co was obtained showing a spherical shape between 54 and 63 nm. Duan *et al.* synthesized an Au@Sm_2O_3 composite by dealloying pure Sm and pure Au at room temperature and later the temperature was elevated to 80 °C and maintained for 10 h.[61] Subsequently, the product was calcined from 300 to 600 for 2 h producing Au@Sm_2O_3 nanorods with a diameter of 10 nm. CO oxidation activity of the synthesized Au@Sm_2O_3 was carried out. In a study by Zhu *et al.* the fabrication of Au/Sm_2O_3 composites *via* a precipitation method was reported.[62] $Sm(NO_3)_3 \cdot 6H_2O$ and Au nanorods were stirred in an aqueous solution containing urea. The reaction solution was heated at 90 °C for 90 min and the product was dried at 90 °C for 3 h. Finally, it was calcined at 600 °C for another 3 h. A co-precipitation method was used to prepare Au@Sm_2O_3 in Yu's work.[63] Au nanorods were mixed together in an aqueous solution of $Sm(NO_3)_3 \cdot 6H_2O$. Urea was added to the mixed solution, which was later heated at 90 °C for 2 h. The product was dried at 60 °C for 12 h and calcined at 900 °C for 4 h to produce monodispersed micro-cubic shaped Au@Sm_2O_3. Rod-like Au@Sm_2O_3 was obtained showing a length of 1.61 μm and a diameter of 928 nm. Barakat *et al.* prepared an Ag@Sm_2O_3 nanocomposite for environmental remediation of cyanide from aqueous solution.[64] $Sm(NO_3)_3 \cdot 6H_2O$ and $Ag(NO_3)$ were mixed with dodecylamine and ethanol and Ag@Sm_2O_3 nanocomposites were produced using a photodeposition technique of the prepared solution at room temperature. The product was dried at 100 °C and calcined at 550 °C for 5 h producing spherical particles.

Preparation of a Sm_2O_3/Cu mosaic structure was reported by Zhang *et al.*[65] The composite was synthesized by mixing and milling both Cu powder and Sm_2O_3 and sintered at 900 °C for 90 min. The infrared absorptivity and emissivity of the product were studied. W/Sm_2O_3 composites were prepared through spark plasma sintering according to Zhu's work.[66] Pure W powder and Sm_2O_3 were mixed and ball milled and sintered at 1600 °C under argon conditions. Intergranular shaped W/Sm_2O_3 was obtained with a particle size between 600 and 800 nm. In another study, W/Sm_2O_3 composites were synthesized using a wet chemical method as reported by Ding *et al.*[67] An aqueous solution of ammonium paratungstate hydrate and $Sm(NO_3)_3 \cdot 6H_2O$ were stirred together at room temperature and dried at 60 °C for 2 h. The final product was calcined at 450 °C for 1 h under a nitrogen atmosphere. A mixture of polygonal and cubic shaped W/Sm_2O_3 composites was obtained. From TEM images, the polygonal shape of W/Sm_2O_3 was less than 20 μm while the cubic composites were about 100 to 150 nm. On the other hand, noble metal NPs offer good thermal stability and strong interaction with rare earth elements. Ullah *et al.* produced Pd NPs decorated on Sm_2O_3 NRs.[68] Firstly, Sm_2O_3 NPs were synthesized using a hydrothermal method in which Pd^{2+} was reduced to Pd^0 *via* photochemical synthesis and decorated on Sm_2O_3 NRs. The average length and width of the NRs were reported to be 120 nm and 22 nm respectively.

Carbon decorated on Sm_2O_3 NPs was prepared in a study done by Chen *et al.*[69] The authors used a sonochemical reaction to prepare the composite utilizing $Sm(NO_3)_3 \cdot 6H_2O$ and CNFs with addition of ammonia solution. The product was dried at 80 °C for 12 h without further calcination treatment producing multi-layered nanofibers and nanospheres. The synthesized materials were used to detect 4-nitrophenol. Carbon nanofiber–Sm_2O_3 nanocomposites have been synthesized and reported by He *et al.*[70] Carbon fibers were dissolved in *N-N*-dimethylformamide solution before the addition of $Sm(NO_3)_3$ and NaOH. The reaction was heated hydrothermally at 120 °C for 24 h. The product was

Table 2 Synthesis of doped Sm_2O_3 and Sm_2O_3-doped metal oxide NPs

No.	Materials	Synthesis method	Particle size	Morphology	Applications	Ref.
1	Co-doped Sm_2O_3	Co-precipitation	13–50 nm	Spherical	—	50
2	Co-doped Sm_2O_3	Combustion	75–90 nm	—	—	51
3	Ni-doped Sm_2O_3	Combustion	107–129 nm	—	—	52
4	Ru-doped Sm_2O_3	Precipitation	100–600 nm	Rod-like	Ammonia decomposition	53
5	Sm_2O_3-doped SnO_2	Combustion	100–300 nm	Agglomerated	Gas sensing	54
6	Sm_2O_3-doped SnO_2	Combustion	50–200 nm	Agglomerated	Gas sensing	55
7	Sm_2O_3-doped SnO_2	Co-precipitation	5–8 nm	—	Acetone sensing	56
8	Sm_2O_3-doped CeO_2	Surfactant assisted microwave	7–22 nm	—	Photodegradation of acid orange 7	57
9	CoO–Sm_2O_3 co-doped SnO_2	Co-precipitation	0.5–3 μm	—	—	58
10	Sm_2O_3-doped ZnO	Hydrothermal	0.5 μm (diameter) and 9–10 μm (length)	—	Nitroaniline chemical sensor	59

treated at 550 °C for 5 h. The synthesized C@Sm_2O_3 composites were applied for novel electrochemical detection of two isomers of dihydroxybenzenes. Ilsemann *et al.* reported on the synthesis of a Ni@Sm_2O_3 xerogel catalyst for CO_2 methanation.[71] The Pechini-PO method was used to produce the Ni@Sm_2O_3 catalyst using $Sm(NO_3)_3·6H_2O$ and $Ni(NO_3)_2$ as the precursors. The reaction solution was stirred at room temperature and the product was dried at room temperature as well. The dried samples were calcined at 600 °C for 2 h producing composites with a crystallite size between 6 and 10 nm.

Boltenkov *et al.* prepared ZnO@Sm_2O_3 using a liquid polymer salt method.[25] In this research, polyvinylpyrrolidone (PVP) was used together with $Zn(NO_3)_2$ and $Sm(NO_3)_3$. The mixed solution was first stirred at room temperature for 15 min before it was thermally treated at 550 °C. Aggregated film-like particles with a particle size less than 100 nm and of 200–250 nm in thickness were obtained. PANI@Sm_2O_3 nanocomposites have been synthesized in a study conducted by Jamnani *et al.*[72] A hydrothermal method was used to fabricate the composite by mixing $Sm(NO_3)_3·6H_2O$ and PANI together in an aqueous solution. A few drops of citric acid were added before it was heated at 180 °C for 24 h. The obtained product was dried at 100 °C for 2 h and calcined at 800 °C for 2 h. Spherical particles of 30–100 nm were obtained. The synthesized PANI@Sm_2O_3 nanocomposites were tested to detect hydrogen at room temperature. A NiO@Sm_2O_3 heterojunction was found to enhance the photo-Fenton activity as stated in Liu's work.[73] NiO@Sm_2O_3 was synthesized *via* a sol gel method in which $Sm(NO_3)_3·6H_2O$ and $Ni(NO_3)_2$ were dissolved and stirred in a solution consisting of citric acid and ethylene glycol. The mixed solution was stirred at room temperature for 2 h before it was heated at 100 °C for 10 h. The obtained gel-like product was calcined at 700 °C for 3 h. Due to their particle size range which is less than 100 nm, the photo-Fenton activity of NiO@Sm_2O_3 was investigated. Pyridoxine analysis of Sm_2O_3 decorated graphitic carbon nitride nanosheets was investigated as reported by Mesgari *et al.*[74] Synthesized Sm_2O_3 NPs were prepared by a sol gel method by mixing $Sm(NO_3)_3$ in polyvinyl alcohol. It was stirred at 90 °C for 2 h and calcined at 400 °C. The obtained Sm_2O_3 and g-C_3N_4 were dispersed in water before they were sonicated and centrifuged. This produced two layers of solution in which a milky layer solution was taken and added to a vortex together with a 1/3 ratio of Sm_2O_3 and g-C_3N_4. The vortexed solution was heated on a hot plate at 45 °C more than 5 times continuously producing spherical particles of g-C_3N_4@Sm_2O_3. Determination of acetaminophen and ciprofloxacin was carried out using Sm_2O_3 nanorod modified graphite as reported by Biswas *et al.*[75] The authors used a sol–gel method to fabricate Sm_2O_3@graphite using poly(ethylene) glycol and NaOH as the solvents. The reaction was done at room temperature for 4 h before it was calcined at 300 to 900 °C for 4 h. The synthesized nanorods were found to be less than 100 nm.

Muneer *et al.* synthesized Gd_2O_3@Sm_2O_3 nanocomposites through sonication and hydrothermal methods.[76] Firstly, $Sm(NO_3)_3·6H_2O$ and $GdCl_3·6H_2O$ were put in a solution containing NaOH and dioctyl sulfosuccinate sodium salt (DSS) which is an anionic surfactant. For the sonochemical method, 100 °C for 120 min was applied, whereas for the hydrothermal method, the solution was heated at 160 °C for 2.5 h. Both products were dried at 100 °C. As for the calcination temperature, Gd_2O_3@Sm_2O_3 synthesized *via* the sonochemical method was calcined at 900 °C for 90 min, while for the hydrothermal method, the product was calcined at 600 °C. Both methods produced a particle size between 15 and 30 nm. Sm_2O_3@ZnO composites have been synthesized by Zeng *et al.* *via* a hydrothermal method.[77] $Sm(NO_3)_3·6H_2O$ and Zn acetate were put in an autoclave with addition of urea, polyvinyl pyrrolidone and ethanol. The reaction was heated at 180 °C for 1 h and the obtained product was dried at 60 °C for 10 h. It was proceeded with calcination at 500 °C for 3 h. Spherical particles were formed with an average particle size of 200 nm. In another study, ZnO@Sm_2O_3 flower-like particles were synthesized *via* microwave assisted synthesis.[78] A solution of $Sm(NO_3)_3·6H_2O$ and Zn acetate was stirred at room temperature and guanidinium carbonate and NaOH were added to the reaction solution. It was then heated in a microwave before the products were dried at 60 °C and calcined at 600 °C for 2 h. The flower-like composites were estimated to be 1.5 μm with well-defined petals of 500–600 nm (Fig. 4).

CuO@Sm_2O_3 nanoflowers were utilized as electrode materials for high performance supercapacitors reported in a study by Zhang *et al.*[79] A co-precipitation method was used to synthesize CuO@Sm_2O_3 in which $Cu(NO_3)_2$ and $Sm(NO_3)_3$ were dissolved in an aqueous solution with addition of ammonia solution. The reaction solution was heated at 150 °C for 6 h and the product was dried at 90 °C for 12 h without further heat treatment. The synthesized CuO@Sm_2O_3 nanoflowers were approximately 2–3 nm. Dezfuli *et al.* synthesized Sm_2O_3@rGO through a sonochemical method.[81] An ammonia solution was added dropwise into an aqueous solution of $Sm(NO_3)_3·6H_2O$ which was then stirred and sonicated for 20 min. A layered and wrinkled Sm_2O_3@rGO composite with an average particle size of 20 nm was obtained. Another study on the synthesis of Sm_2O_3@rGO was reported by Reddy *et al.*[82] The synthesis was done using an eggshell membrane assisted hydrothermal route. The reaction was heated at 180 °C for 24 h and calcined at 800 °C. Sm_2O_3@rGO nanorods were 10 nm in diameter and 60 to 120 nm long. The room temperature LPG detection properties of the Sm_2O_3@rGO nanorods were studied. Similarly, Sm_2O_3@rGO was prepared by a facile sonochemical route.[83] They were synthesized individually. For instance, Sm_2O_3 was prepared hydrothermally while rGO was prepared using a modified Hummers method. Then, in order to prepare Sm_2O_3@rGO nanocomposites, RGO and Sm_2O_3 were dispersed in DMF solution and sonicated for 1 h.

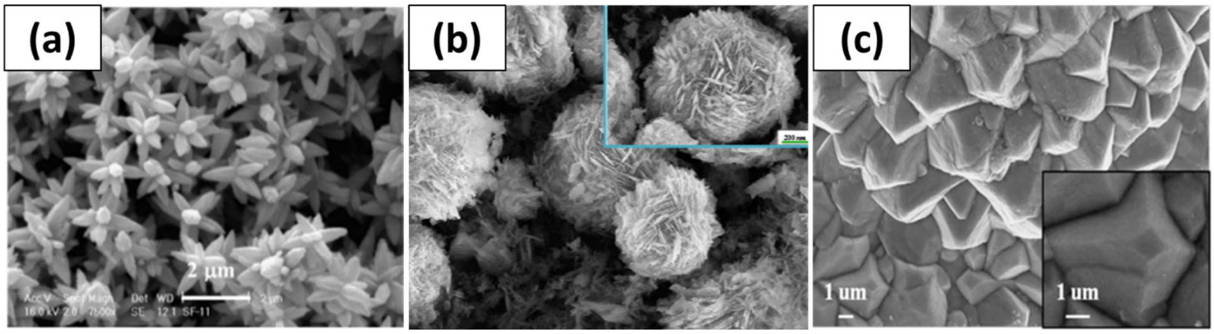

Fig. 4 SEM images of (a) flower-like ZnO@Sm_2O_3, (b) flower-like CuO@Sm_2O_3 and (c) pyramid-like Ti/PbO_2@Sm_2O_3.[78–80] Figure (a) has been adapted from ref. 78 with permission from *Sensors and Actuators B: Chemical*, copyright 2023, figure (b) has been adapted from ref. 79 with permission from *Applied Surface Science*, copyright 2023, and figure (c) has been adapted from ref. 80 with permission from *Journal of Colloid and Interface Science*, copyright 2023.[78–80]

Li *et al.* synthesized Sm_2O_3@ZrO_2 composites using $ZrOCl_2$ and $Sm(NO_3)_3·6H_2O$ *via* co-precipitation.[84] The synthesis reaction was carried out at room temperature and the product was dried at 100 °C for 24 h, followed by subsequent calcination at 600 °C for 3 h. Sm_2O_3@ZrO_2 composites were formed with a crystallite size between 5 and 15 nm. Sm_2O_3-modified TiO_2 nanotubes were prepared through a hydrothermal reaction as reported by Liu *et al.*[85] Ammonium fluoride, ethylene glycol, $Sm(NO_3)_3$ and titanium foil were mixed and stirred at room temperature before they were heated at 100 °C for 12 h hydrothermally. The product was annealed at 550 °C for 1 h producing 13 μm nanotubes.

Sm_2O_3@CeO_2-supported Pd catalysts have been synthesized using a ball milling method.[86] Commercially available Sm_2O_3, CeO_2 and Pd NPs were ball-milled together and heated at 800 °C for 2 h. The product was then annealed at 800 °C for 2 h. In another study, Sm_2O_3@CeO_2-supported Pd catalysts were also synthesized using the same synthesis method.[87] The product was calcined at 800 °C for 2 h as well. A mixture of rounded and irregular particles was obtained and the composites were used for intermediated-temperature methanol fuel cells. ZnS–ZnO–Sm_2O_3 composites were used for photocatalytic removal of dyes and antibiotics in the visible light region as reported by Zheng *et al.*[88] ZnS–ZnO–Sm_2O_3 composites were synthesized hydrothermally by mixing $Sm(NO_3)$, $Zn(NO_3)_2$ and ZnS with urea PVP and ethanol. The reaction was heated at 180 °C for 1 h and the product was dried at 50 °C for 10 h. The final product was then calcined at 300 °C for 2 h producing 10 nm size spherical particles. Zhang *et al.* in their work reported on the synthesis of Ti/PbO_2@Sm_2O_3 composites for highly efficient electrocatalytic degradation of alizarin yellow R.[80] The composites were prepared *via* a simple electrodeposition technique. The electrode was deposited at 65 °C and dried in air after the deposition was finished. Pyramid-like microparticles were observed in the SEM image. Mesoporous NiO–Sm_2O_3/Al_2O_3 catalysts have been prepared using a one-pot EISA method according to a study conducted by Liu *et al.*[89] The composite precursors were vigorously stirred at room temperature for 5 h and the solvents used in this preparation were evaporated at 60 °C. After that, the obtained product was calcined at 550 °C for 4 h, producing 3–5 nm particles. Ordered mesoporous silica loaded with Sm_2O_3 was also prepared using a one step sol gel method.[90] The reaction was aged for 20 h and dried at 50 °C. The product was finally calcined at 800 °C for 2 h. Well-organized and large mesoporous channel-like particles were obtained which were about 600 nm to 1 μm. Ayub *et al.* prepared barium promoted Ni/Sm_2O_3 to enhance the CO_2 methanation process.[91] A wetness impregnation method was used to synthesize the material in which a mixture of Ba^{2+}, Ni^{2+} salts and Sm_2O_3 was stirred continuously for 3 h at 60 °C to ensure thorough dispersion. The catalysts were dried at 200 °C for 2 h and calcined at 500 °C for 3 h producing groundnut-shaped Ni–Ba/Sm_2O_3. Below is the summary of synthesis methods used to synthesize Sm_2O_3-based materials (Table 3).

In summary, Sm_2O_3, doped-Sm_2O_3 and Sm_2O_3-based materials have been fabricated in various ways (Fig. 5). Different synthesis method parameters have been considered to direct the shapes and properties of Sm_2O_3 hence affecting the final physical, optical and chemical properties of Sm_2O_3, doped-Sm_2O_3 and Sm_2O_3-based materials. It is known that the properties of metal oxides would influence the response in various applications in which it will be discussed in the next section.

5.0. Applications of Sm_2O_3 and Sm_2O_3-based materials

Sm_2O_3 and Sm_2O_3-based materials have been applied in various fields.[93–96] Different structures, morphologies and particle sizes will lead to different activities of Sm_2O_3. Therefore, in this section, the application activities of Sm_2O_3 and Sm_2O_3-based materials that have been synthesized using different synthesis methods were discussed (Fig. 6).

5.1. Photocatalytic removal of organic pollutants

There are two types of organic pollutants that have been a threat to the environment and marine lives, which are

Table 3 Synthesis methods used to prepare Sm_2O_3-based materials

No.	Materials	Synthesis methods	Particle size	Morphology	Application	Ref.
1	$Co@Sm_2O_3$	Wet impregnation	54–63 nm	Spherical	CO_2 reforming	60
2	$Au@Sm_2O_3$	Dealloying	10 nm	Rod-like	CO oxidation	61
3	$Au@Sm_2O_3$	Precipitation	1.61 μm (length) and 928 nm (diameter)	Rod-like	—	62
4	$Au@Sm_2O_3$	Co-precipitation	—	Cubic	Photothermal conversion	63
5	$Ag@Sm_2O_3$	Photodeposition	—	Spherical	Cyanide removal	64
6	$Cu@Sm_2O_3$	Milling	—	Mosaic	—	65
7	$W@Sm_2O_3$	Spark plasma sintering	600–800 nm	Intergranular	—	66
8	$W@Sm_2O_3$	Spark plasma sintering	Polygonal– 20 μm Cubic – 100–150 nm	Polygonal and cubic	—	67
9	$Pd@Sm_2O_3$	Hydrothermal and photochemical	120 nm (length) and 22 nm (width)	Rod-like	—	68
10	$C@Sm_2O_3$	Sonochemical	—	Fiber and sphere-like	4-Nitrophenol detection	92
11	$C@Sm_2O_3$	Hydrothermal	—	—	Detection of isomers	70
12	$ZnO@Sm_2O_3$	Liquid polymer salt	100 nm and 200–250 nm (thickness)	Film-like	—	25
13	$PANI@Sm_2O_3$	Hydrothermal	30–100 nm	Spherical	Hydrogen detection	72
14	$NiO@Sm_2O_3$	Sol–gel	Less than 100 nm	—	Photo-Fenton activity	73
15	$g-C_3N_4@Sm_2O_3$	Sonication	—	Spherical	—	74
16	Sm_2O_3@graphite	Sol–gel	Less than 100 nm	Rod-like	Determination of acetaminophen and ciprofloxacin	75
17	$Gd_2O_3@Sm_2O_3$	Sonication and hydrothermal	15–30 nm	—	—	76
18	$Sm_2O_3@ZnO$	Hydrothermal	200 nm	Spherical	—	77
19	$Sm_2O_3@ZnO$	Microwave-assisted	1.5 μm with well-defined petals of 500–600 nm	Flower like	—	78
20	$CuO@Sm_2O_3$	Co-precipitation	2–3 nm	Flower-like	Supercapacitor	79
21	Sm_2O_3@rGO	Sonochemical	20 nm	Wrinkled	—	81
22	Sm_2O_3@rGO	ESM assisted hydrothermal	10 nm (diameter) and 60–120 nm (length)	Rod-like	LPG detection	82
23	Sm_2O_3@RGO	Sonochemical	∼30–40 nm	Rod-like and wrinkle-like	Carbendazim detection	83
24	$Sm_2O_3@ZrO_2$	Co-precipitation	5–15 nm	—	—	84
25	$Sm_2O_3@TiO_2$	Hydrothermal	13 μm	Tube-like	—	85
26	$Sm_2O_3@CeO_2$-supported Pd	Ball milling	—	—	—	86
27	$Sm_2O_3@CeO_2$-supported Pd	Ball milling	—	A mixture of irregular and round	Methanol fuel cells	87
28	$ZnS–ZnO–Sm_2O_3$	Hydrothermal	10 nm	Spherical	Photocatalytic dye and antibiotic removal	88
29	$Ti/PbO_2@Sm_2O_3$	Electrodeposition	—	Pyramid-like	Photocatalytic degradation of alizarin yellow R	80
30	$NiO–Sm_2O_3/Al_2O_3$	One-pot EISA	3–5 nm	—	—	89
31	$Silica@Sm_2O_3$	Sol–gel	600 nm to 1 μm	Channel-like	—	90
32	$Ni–Ba/Sm_2O_3$	Wetness impregnation	—	Groundnut	CO_2 methanation	91

coloured and non-coloured pollutants. Examples of coloured pollutants are dyes while non-coloured pollutants are toxic chemicals that are colourless such as metals. In a study conducted by Jourshabani *et al.*, the activities of Sm_2O_3 and Sm_2O_3@CNS in photocatalytic degradation of methylene blue (MB) under visible light were reported.[97] Pure Sm_2O_3 was found to degrade only up to 57% of MB in 150 min. Remarkably, Sm_2O_3@CNS illustrated the best photocatalytic performance of 92.6% under visible light irradiation for 150 min. The less enhanced photocatalytic degradation of MB using pure Sm_2O_3 might be due to the wide band gap of Sm_2O_3 which is about 4.3 eV.[98] Metal oxides are known to be important semiconductor photocatalysts due to their stabilities and their remarkable properties. However, one of the major drawbacks is their inactivity under visible light irradiation.[99] Therefore, to minimize the drawbacks, doping or producing Sm_2O_3 composites is opted. In this study, dye molecules were anchored on the photocatalyst surface as the surface area of the composites was improved due to the combination of Sm_2O_3 with CNS. Besides, the heterojunction formation in Sm_2O_3@CNS composites also increases the recombination lifetime of electron–hole pairs by the depletion layer region.

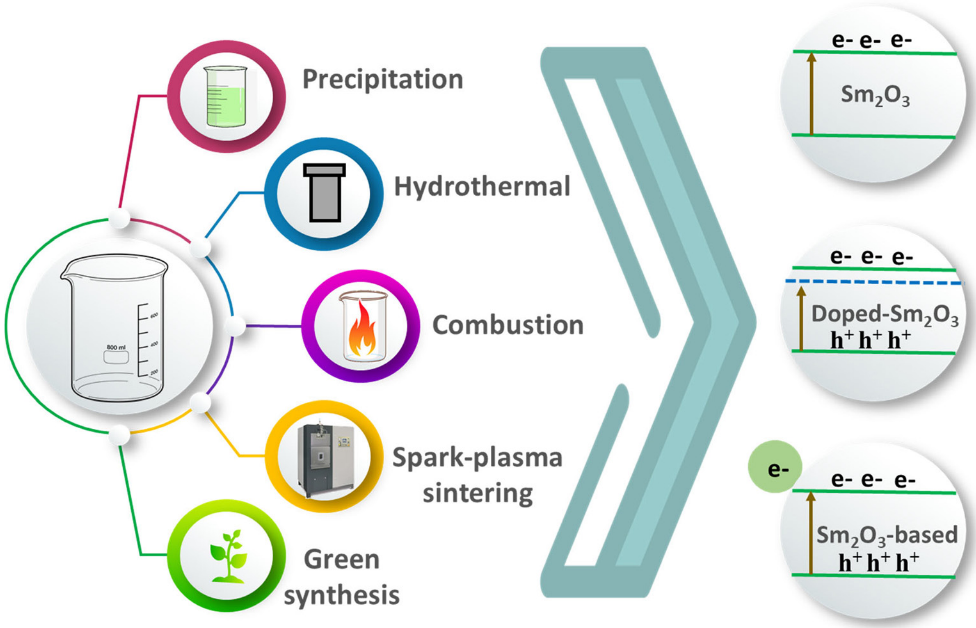

Fig. 5 Common synthesis methods used to synthesize Sm_2O_3, doped-Sm_2O_3 and Sm_2O_3-based materials.

Interesting findings were observed in a report by Zheng *et al.* in which the effect of binary and ternary composites on the photocatalytic degradation of TCH, rhodamine B (RhB), methyl orange and methylene blue was investigated.[88] The photocatalytic activities of ternary (ZnS–ZnO–Sm_2O_3) and binary ZnO–Sm_2O_3 were reported to be influenced by both $^{\bullet}OH$ and $^{\bullet}O_2^-$ radicals.[100] Based on their findings, the enhancement in the photocatalytic activities also showed efficient charge transfer and high resistance to the recombination of charge carriers.[101] However, the separation of e^-/h^+ of the ternary ZnS–ZnO–Sm_2O_3 junction is more efficient than that of binary ZnO–Sm_2O_3. In Fig. 7, the electrons in the CB of Sm_2O_3 are transferred to that of ZnS, which are further transferred to that of ZnO in the ZnS–ZnO–Sm_2O_3 junction. Meanwhile, h^+ in the VB of Sm_2O_3 and ZnO are transferred to that of ZnS (Fig. 7).[102,103] One should note that the excess amount of Sm_2O_3 will only hinder the light absorption in the visible region due to its wide band gap, which leads to the inferior quantum efficiency of ZnS–ZnO–Sm_2O_3. Similar findings were also reported elsewhere.[80,88,104]

5.2. Sm_2O_3 and Sm_2O_3-based materials as sensors

Sm_2O_3 and Sm_2O_3-based materials have been reported to be used as sensors *i.e.*, chemical and gas sensors. For

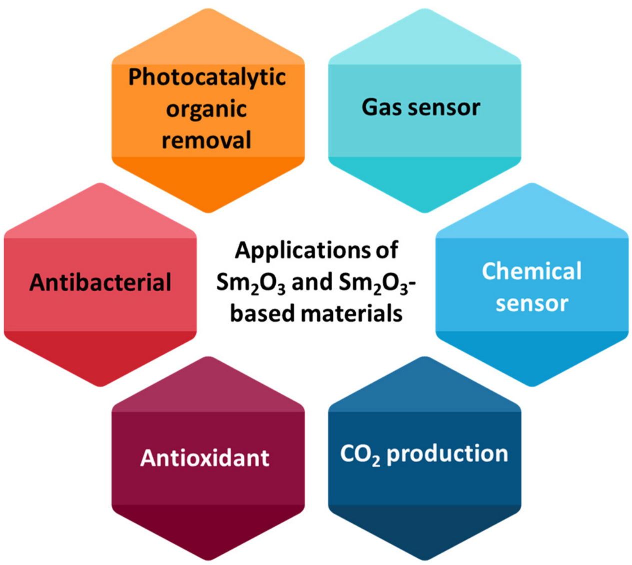

Fig. 6 Reported applications of Sm_2O_3 and Sm_2O_3-based materials.

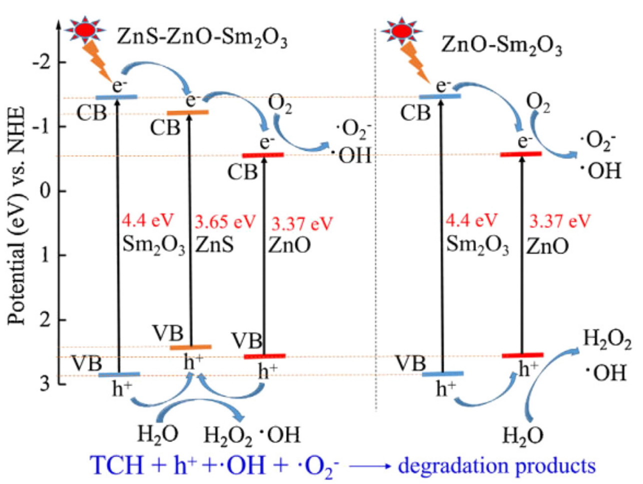

Fig. 7 The mechanism of ZnS–ZnO–Sm_2O_3 composites in photocatalytic degradation of organic pollutants.[88] This figure has been adapted from ref. 88 with permission from *Journal of Industrial and Engineering Chemistry*, copyright 2023.[88]

instance, Yan *et al.* reported a novel electrode material used in enzyme-free electrochemical detection of H_2O_2 using Sm_2O_3 hydrangea microspheres.[41] The Sm_2O_3 hydrangea microsphere electrode exhibited excellent performance which showed the following characteristics: detection linear range from 1 to 320 μM (R^2 = 0.997), ultrahigh sensitivity of 20.5 μA mM^{-1}, low detection limit of ~1 μM, fast response at 3 s to attain 95% of the steady current as well as high stability. These remarkable properties were attributed to the large specific surface area of the mesoporous Sm_2O_3, which ensures efficient mass transport as well as the sensitivity of the Sm_2O_3 for the H_2O_2 electro-reduction reaction. In another study, Teker *et al.* studied the detection of paracetamol using sensitive and selective Sm_2O_3@ZrO_2@CNT composites.[105] Large enhancement in the magnitude of the peak response for paracetamol was observed using the proposed electrode. Interestingly, selective detection of paracetamol was successful as no interference of ascorbic acid and tramadol was observed. The selectivity property of the composites might be due to the high conductivity and excellent catalytic activity of Sm_2O_3 NPs. Furthermore, a composite electrode with samarium provides thermal and chemical stability and large surface area.[81,106,107] Detection of 4-nitrophenol was carried out using Sm_2O_3 NPs decorated with carbon nanofibers.[92] It was found that trace levels of 4-NP can be detected by the Sm_2O_3@carbon nanofiber modified electrode which showed the best sensitivity. In addition, the sensor also displayed excellent anti-interference ability. This may be attributed to the synergistic influence of the sensing substrate. Similar findings were also found in the literature.[59,108]

Additionally, Sm_2O_3-based materials have been used as gas sensors, for example, a recent study was conducted by Reddy *et al.* on the detection of LPG at room temperature using Sm_2O_3/rGO.[82] According to their findings, the Sm_2O_3/rGO hybrid flexible sensor offers the highest sensitivity with a maximum response of 116% under comfort humidity zone. Moreover, it showed excellent stability even after mechanical bending towards 700 ppm of LPG at room temperature. In another study, Sm_2O_3 was combined with SnO_2 to detect the presence of C_2H_2.[109] The composites have a significant impact on enhancing the sensitivity properties of individual Sm_2O_3 and SnO_2 sensors to C_2H_2 gas. This property might be due to the increasing active centers on SnO_2 by Sm_2O_3. Furthermore, the addition of Sm^{3+} might change the electronic movement and the overlap of electron cloud of the SnO_2 material resulting in the strengthening of the electronegativity of the carbon–hydrogen triple bond of C_2H_2. This eventually makes it easier for hydrogen dissociation to combine with O^{2-}. The amount of active centers present might influence the sensing ability in reduced particle size, *i.e.* a high surface area provides more active sites for oxygen adsorption and quick channels for gas adsorption.[110] Similar findings can be found in other literature reports.[32,54,55,111,112]

5.3. Photocatalytic CO_2 conversion

One study conducted by Gómez-Sainero *et al.* reported on the production of CO_2 from methanol conversion using Sm_2O_3@CeO_2@Pd.[86] According to the authors, CO_2 was produced either by the direct reforming of methanol or by the subsequent transformation of CO *via* the water gas-shift reaction. Moreover, in a recent study, the potential of greenhouse gas abatement *via* catalytic methane dry reforming using Co@Sm_2O_3 catalysts was investigated.[60] The 20 wt% Co/80 wt% Sm_2O_3 catalyst produced the highest CH_4 and CO_2 conversion of ~71 and ~74% as well as the highest hydrogen (H_2) and carbon monoxide (CO) yield of ~62 and ~73%, respectively. Duan *et al.* studied the activities of Au/Sm_2O_3 catalysts for low-temperature CO oxidation.[61] The catalyst prepared with 0.5 at% Au/Sm_2O_3 exhibited the best catalytic activity and could convert 35% of CO at room temperature (20 °C).

5.4. Photocatalytic production of organic compounds

Sm_2O_3-based materials have also been used as catalysts to prepare organic compounds. For instance, Maddila *et al.* used Sm_2O_3@fluoroapatite as a catalyst to prepare triazolidine-3-thione derivatives under green solvent conditions yielding about 92–97% products. The reaction was carried out at room temperature for about 20 to 45 min depending on the catalysts used in the reaction. Furthermore, in a recent study, synthesis of 2-azidoalcohol was carried out using sweet-corn like Sm_2O_3.[36] It was found that, with addition of the catalyst, around 97% of *trans*-2-azidocyclohexanol was yielded as compared to that without a catalyst with only 27% production. This showed that the Sm_2O_3 sweet corns could lead to a highly active Brønsted acid catalyst that can produce excellent yields for 1,2-azidoalcohol.

5.5. Biological applications

Sm_2O_3 NPs have been used as antibacterial and antioxidant agents in a study reported by Muthulakshmi *et al.*[39] Sm_2O_3 NPs were used against *S. aureus* and *E. coli* in which the activities showed zones of inhibition between 15 and 17 mm and 17 and 22 nm, respectively. According to the authors, the higher zone of inhibition against *E. coli* might be due to the decay of cell membranes in *E. coli* with cell elongation by oxidative stress leading to bacterial cell death. Moreover, the *E. coli* and *S. aureus* bacterial systems absorbed the released cations. The absorbed cations bind to the surface of the bacterial systems causing release of cellular materials from the *E. coli* and *S. aureus* bacterial systems.[113,114] Two possible antibacterial mechanisms are reported by Kokilavani *et al.*[115] First, the antibacterial activity might be due to the direct encounter of NPs with bacterial cells and the second mechanism might be due to the interaction of subordinate products. Furthermore, Muthulakshmi *et al.* also investigated the antioxidant activities of Sm_2O_3 NPs using a DPPH antioxidant assay. The activities increased as the concentration of Sm_2O_3 increased, *i.e.*, 14.33 to 85.23% from 10 μg mL^{-1} to 100 μg mL^{-1}.[39] The leaf extract used in the synthesis of Sm_2O_3 NPs was responsible for the enhancement of the antioxidant activity. Besides, the antioxidant activity was also increased due to ROS generation which leads to cell death.[116,117] On the other hand, Sm_2O_3 nanoplatelets were used as a biosensor of glucose oxidase in a study conducted by Leote *et al.*[48] The glucose biosensor based on Sm_2O_3 was tested for glucose detection in serum samples with a recovery factor of 90%. The electrocatalytic behavior of Sm_2O_3 towards H_2O_2 generation allows sensitive detection of the products from enzymatic reactions. This property is unusual for oxide-based biosensors due to the potential applicability towards the analysis of biological fluids with high complexity, such as blood serum.

6.0. Future prospects

Comprehensive framework syntheses have been reported in the literature. However, there are a few research gaps that still need to be filled.

i. The syntheses of Sm_2O_3 NPs have been reported. However, more research should be conducted on the synthesis of Sm_2O_3 NPs *via* various synthesis methods.

ii. The properties of Sm_2O_3 and Sm_2O_3-based materials have not been investigated thoroughly.

iii. The applications of Sm_2O_3 and Sm_2O_3-based materials have not been widely studied.

iv. Interaction of Sm_2O_3 and Sm_2O_3-based materials with pollutants, gases, chemicals, *etc.* in applications should be explained in detail.

v. Sm_2O_3 has great potential as a dielectric material. However, there is a lack of study on it being a potentially good dielectric material.

7.0. Conclusion

Sm_2O_3 recently has been brought to the attention of researchers as it possesses unique physical and chemical properties. In this review, the syntheses of Sm_2O_3 and Sm_2O_3-based materials using precipitation, hydrothermal, green synthesis, combustion, *etc.* were discussed. The properties and morphologies of the synthesized Sm_2O_3 and Sm_2O_3-based materials were also reported. The investigation of the synthesized Sm_2O_3 and Sm_2O_3-based materials for applications such as photocatalytic dye degradation, removal of toxic chemical pollutants, and gas sensors as well as antibacterial activities was discussed.

Author contributions

Mohammad Mansoob Khan: supervision, conceptualization, funding acquisition, writing – review & editing. Shaidatul Najihah Matussin: methodology, investigation, data curation, writing – original draft.

Conflicts of interest

The authors declared no conflicts of interest.

Acknowledgements

The authors would like to acknowledge the FRC grant (UBD/RSCH/1.4/FICBF(b)/2022/046) received from Universiti Brunei Darussalam, Brunei Darussalam.

References

1 I. Khan, K. Saeed and I. Khan, Nanoparticles: Properties, Applications and Toxicities, *Arabian J. Chem.*, 2019, **12**(7), 908–931, DOI: **10.1016/j.arabjc.2017.05.011**.

2 M. Sternik and U. D. Wdowik, Probing the Impact of Magnetic Interactions on the Lattice Dynamics of Two-Dimensional Ti2X (X = C, N) MXenes, *Phys. Chem. Chem. Phys.*, 2018, **20**(11), 7754–7763, DOI: **10.1039/c7cp08270c**.

3 S. N. Matussin, A. Rahman and M. M. Khan, Role of Anions in the Synthesis and Crystal Growth of Selected Semiconductors, *Front. Chem.*, 2022, **10**, 881518, DOI: **10.3389/fchem.2022.881518**.

4 M. M. Khan, S. F. Adil and A. Al-Mayouf, Metal Oxides as Photocatalysts, *J. Saudi Chem. Soc.*, 2015, **19**(5), 462–464, DOI: **10.1016/j.jscs.2015.04.003**.

5 Z. N. Kayani, Maria, S. Riaz and S. Naseem, Magnetic and Antibacterial Studies of Sol-Gel Dip Coated Ce Doped TiO2 Thin Films: Influence of Ce Contents, *Ceram. Int.*, 2020, **46**(1), 381–390, DOI: **10.1016/j.ceramint.2019.08.272**.

6 S. Chen, X. Zhao, H. Xie, J. Liu, L. Duan, X. Ba and J. Zhao, Photoluminescence of Undoped and Ce-Doped SnO2thin Films Deposited by Sol-Gel-Dip-Coating Method, *Appl. Surf. Sci.*, 2012, **258**(7), 3255–3259, DOI: **10.1016/j.apsusc.2011.11.077**.

7 S. P. Radhika, K. J. Sreeram and B. Unni Nair, Mo-Doped Cerium Gadolinium Oxide as Environmentally Sustainable Yellow Pigments, *ACS Sustainable Chem. Eng.*, 2014, **2**(5), 1251–1256, DOI: **10.1021/sc500085m**.

8 P. Moontragoon, S. Pinitsoontorn and P. Thongbai, Mn-Doped ZnO Nanoparticles: Preparation, Characterization, and Calculation of Electronic and Magnetic Properties, *Microelectron. Eng.*, 2013, **108**(3), 158–162, DOI: **10.1016/j.mee.2013.01.061**.

9 Z. Xiong, Z. Lei, Z. Xu, X. Chen, B. Gong, Y. Zhao, H. Zhao, J. Zhang and C. Zheng, Flame Spray Pyrolysis Synthesized ZnO/CeO2 Nanocomposites for Enhanced CO2 Photocatalytic Reduction under UV-Vis Light Irradiation, *J. CO2 Util.*, 2017, **18**, 53–61, DOI: **10.1016/j.jcou.2017.01.013**.

10 V. G. Nair, R. Jayakrishnan, J. John, J. A. Salam, A. M. Anand and A. Raj, Anomalous Photoconductivity in Chemical Spray Pyrolysis Deposited Nano-Crystalline ZnO Thin Films, *Mater. Chem. Phys.*, 2020, **247**(December 2019), 122849, DOI: **10.1016/j.matchemphys.2020.122849**.

11 N. Bhuvanendran, S. Ravichandran, S. Kandasamy, W. Zhang, Q. Xu, L. Khotseng, T. Maiyalagan and H. Su, Spindle-Shaped CeO2/Biochar Carbon with Oxygen-Vacancy

as an Effective and Highly Durable Electrocatalyst for Oxygen Reduction Reaction, *Int. J. Hydrogen Energy*, 2021, **46**(2), 2128–2142, DOI: 10.1016/j.ijhydene.2020.10.115.
12 S. Zhao, D. Kang, Y. Liu, Y. Wen, X. Xie, H. Yi and X. Tang, Spontaneous Formation of Asymmetric Oxygen Vacancies in Transition-Metal-Doped CeO2Nanorods with Improved Activity for Carbonyl Sulfide Hydrolysis, *ACS Catal.*, 2020, **10**(20), 11739–11750, DOI: 10.1021/acscatal.0c02832.
13 T. Gaudisson, R. Sayed-Hassan, N. Yaacoub, G. Franceschin, S. Nowak, J. M. Grenèche, N. Menguy, P. Sainctavit and S. Ammar, On the Exact Crystal Structure of Exchange-Biased Fe3O4-CoO Nanoaggregates Produced by Seed-Mediated Growth in Polyol, *CrystEngComm*, 2016, **18**(21), 3799–3807, DOI: 10.1039/c6ce00700g.
14 P. P. Goswami, H. A. Choudhury, S. Chakma and V. S. Moholkar, Sonochemical Synthesis of Cobalt Ferrite Nanoparticles, *Int. J. Chem. Eng.*, 2013, **2013**, 934234, DOI: 10.1155/2013/934234.
15 H. J. Liu and Y. C. Zhu, Synthesis and Characterization of Ternary Chalcogenide ZnCdS 1D Nanostructures, *Mater. Lett.*, 2008, **62**(2), 255–257, DOI: 10.1016/j.matlet.2007.05.011.
16 A. Akah, Application of Rare Earths in Fluid Catalytic Cracking: A Review, *J. Rare Earths*, 2017, **35**(10), 941–956, DOI: 10.1016/S1002-0721(17)60998-0.
17 S. N. Matussin, M. H. Harunsani and M. M. Khan, CeO2 and CeO2-Based Nanomaterials for Photocatalytic, Antioxidant and Antimicrobial Activities, *J. Rare Earths*, 2022, **41**(2), 167–181, DOI: 10.1016/j.jre.2022.09.003.
18 H. Xiao, P. Li, F. Jia and L. Zhang, General Nonaqueous Sol-Gel Synthesis of Nanostructured Sm 2 O 3 , Gd 2 O 3, Dy 2 O 3, and Gd 2 O 3 : Eu 3 + Phosphor, *J. Phys. Chem. C*, 2009, 0–7.
19 C. Barad, G. Kimmel, H. Hayun, D. Shamir and K. Hirshberg, Phase stability of nanocrystalline grains of rare-earth oxides (Sm2O3 and Eu2O3) confined in magnesia (MgO) matrix, *Materials*, 2020, **13**(9), 2201.
20 H. Kohlmann, The Crystal Structure of Cubic C -Type Samarium Sesquioxide, Sm 2 O 3, *Z. Naturforsch. B*, 2019, **74**(5), 433–435, DOI: 10.1515/znb-2019-0042.
21 H. Iwai, S. Ohmi, S. Akama, C. Ohshima, A. Kikuchi, I. Kashiwagi, J. Taguchi, H. Yamamoto, J. Tonotani, Y. Kim, I. Ueda, A. Kuriyama and Y. Yoshihara, Advanced Gate Dielectric Materials for Sub-100 Nm CMOS, in *Digest. International Electron Devices Meeting*, IEEE, 2003, pp. 625–628, DOI: 10.1109/IEDM.2002.1175917.
22 M. Houssa, L. Pantisano, L.-Å. Ragnarsson, R. Degraeve, T. Schram, G. Pourtois, S. De Gendt, G. Groeseneken and M. M. Heyns, Electrical Properties of High-κ Gate Dielectrics: Challenges, Current Issues, and Possible Solutions, *Mater. Sci. Eng. R Rep.*, 2006, **51**(4–6), 37–85, DOI: 10.1016/j.mser.2006.04.001.
23 O. Engström, B. Raeissi, S. Hall, O. Buiu, M. C. Lemme, H. D. B. Gottlob, P. K. Hurley and K. Cherkaoui, Navigation Aids in the Search for Future High-k Dielectrics: Physical and Electrical Trends, *Solid-State Electron.*, 2007, **51**(4), 622–626, DOI: 10.1016/j.sse.2007.02.021.
24 X. He, F. Ye, H. Zhang and L. Liu, Effect of Sm2O3 Content on Microstructure and Thermal Conductivity of Spark Plasma Sintered AlN Ceramics, *J. Alloys Compd.*, 2009, **482**(1–2), 345–348, DOI: 10.1016/j.jallcom.2009.04.013.
25 I. S. Boltenkov, E. V. Kolobkova and S. K. Evstropiev, Synthesis and Characterization of Transparent Photocatalytic ZnO-Sm2O3 and ZnO-Er2O3 Coatings, *J. Photochem. Photobiol., A*, 2018, **367**, 458–464, DOI: 10.1016/j.jphotochem.2018.09.016.
26 S. Devendiran and D. Sastikumar, Fiber Optic Gas Sensor Based on Light Detection from the Samarium Oxide Clad Modified Region, *Opt. Fiber Technol.*, 2018, **46**(September), 215–220, DOI: 10.1016/j.yofte.2018.10.014.
27 T. D. Nguyen, D. Mrabet and T. O. Do, Controlled Self-Assembly of Sm2O3 Nanoparticles into Nanorods: Simple and Large Scale Synthesis Using Bulk Sm2O 3 Powders, *J. Phys. Chem. C*, 2008, **112**(39), 15226–15235, DOI: 10.1021/jp804030m.
28 Y. Cheng, H. Nan, Q. Li, Y. Luo and K. Chu, A Rare-Earth Samarium Oxide Catalyst for Electrocatalytic Nitrogen Reduction to Ammonia, *ACS Sustainable Chem. Eng.*, 2020, **8**(37), 13908–13914, DOI: 10.1021/acssuschemeng.0c05764.
29 R. Mohammadinasab, M. Tabatabaee, H. Aghaie and M. A. Seyed Sadjadi, A Simple Method for Synthesis of Nanocrystalline Sm2O3 Powder by Thermal Decomposition of Samarium Nitrate, *Synth. React. Inorg., Met.-Org., Nano-Met. Chem.*, 2014, **45**(3), 451–454, DOI: 10.1080/15533174.2013.819912.
30 S. B. Ubale, T. T. Ghogare, V. C. Lokhande, T. Ji and C. D. Lokhande, Electrochemical Behavior of Hydrothermally Synthesized Porous Groundnuts-like Samarium Oxide Thin Films, *SN Appl. Sci.*, 2020, **2**, 756, DOI: 10.1007/s42452-020-2467-z.
31 S. R. Jamnani, H. M. Moghaddam, S. G. Leonardi and G. Neri, A Novel Conductometric Sensor Based on Hierarchical Self-Assembly Nanoparticles Sm2O3 for VOCs Monitoring, *Ceram. Int.*, 2018, **44**(14), 16953–16959, DOI: 10.1016/j.ceramint.2018.06.136.
32 C. R. Michel, A. H. Martínez-Preciado, R. Parra, C. M. Aldao and M. A. Ponce, Novel CO2 and CO Gas Sensor Based on Nanostructured Sm 2O3 Hollow Microspheres, *Sens. Actuators, B*, 2014, **202**, 1220–1228, DOI: 10.1016/j.snb.2014.06.038.
33 S. Rasouli Jamnani, H. Milani Moghaddam, S. G. Leonardi, N. Donato and G. Neri, Synthesis and Characterization of Sm2O3 Nanorods for Application as a Novel CO Gas Sensor, *Appl. Surf. Sci.*, 2019, **487**(December 2018), 793–800, DOI: 10.1016/j.apsusc.2019.05.124.
34 J. G. Kang, B. K. Min and Y. Sohn, Synthesis and Characterization of Sm(OH)3 and Sm2O3 Nanoroll Sticks, *J. Mater. Sci.*, 2015, **50**(4), 1958–1964, DOI: 10.1007/s10853-014-8760-8.
35 B. T. Sone, E. Manikandan, A. Gurib-Fakim and M. Maaza, Sm2O3 Nanoparticles Green Synthesis via Callistemon

Viminalis' Extract, *J. Alloys Compd.*, 2015, **650**, 357–362, DOI: 10.1016/j.jallcom.2015.07.272.

36 A. H. Tamboli and H. Kim, Facile Synthesis of Sweet Corn like Sm2O3 and Their Catalytic Performance for 2-Azidoalcohol Synthesis, *Colloids Surf., A*, 2017, **535**(July), 121–129, DOI: 10.1016/j.colsurfa.2017.09.033.

37 L. Yin, D. Zhang, J. Ma, D. Wang, Z. Liang, J. Huang and H. Zhang, Self-Assembly of 3D Hierarchical Clew-like Sm2O3 Microspheres, *Mater. Lett.*, 2016, **183**(41), 401–404, DOI: 10.1016/j.matlet.2016.07.057.

38 L. Yin, D. Wang, J. Huang, G. Tan and H. Ren, Controllable Synthesis of Sm2O3 Crystallites with the Assistance of Templates by a Hydrothermal-Calcination Process, *Mater. Sci. Semicond. Process.*, 2015, **30**, 9–13, DOI: 10.1016/j.mssp.2014.09.034.

39 V. Muthulakshmi, M. Balaji and M. Sundrarajan, Biomedical Applications of Ionic Liquid Mediated Samarium Oxide Nanoparticles by Andrographis Paniculata Leaves Extract, *Mater. Chem. Phys.*, 2020, **242**, 122483, DOI: 10.1016/j.matchemphys.2019.122483.

40 M. A. Ruiz-Gómez, C. Gómez-Solís, M. E. Zarazúa-Morín, L. M. Torres-Martínez, I. Juárez-Ramírez, D. Sánchez-Martínez and M. Z. Figueroa-Torres, Innovative Solvo-Combustion Route for the Rapid Synthesis of MoO 3 and Sm2O3 Materials, *Ceram. Int.*, 2014, **40**(1 PART B), 1893–1899, DOI: 10.1016/j.ceramint.2013.07.095.

41 Y. Yan, K. Li, Y. Dai, X. Chen, J. Zhao, Y. Yang and J. M. Lee, Synthesis of 3D Mesoporous Samarium Oxide Hydrangea Microspheres for Enzyme-Free Sensor of Hydrogen Peroxide, *Electrochim. Acta*, 2016, **208**, 231–237, DOI: 10.1016/j.electacta.2016.05.037.

42 T. Yu, J. Joo, Y. I. Park and T. Hyeon, Single Unit Cell Thick Samaria Nanowires and Nanoplates, *J. Am. Chem. Soc.*, 2006, **128**(6), 1786–1787, DOI: 10.1021/ja057264b.

43 J. F. Huang, Y. Huang, L. Y. Cao and J. P. Wu, Influence of Hydrothermal Reaction Time on Phases, Morphologies and Optical Properties of Sm2O3 Thin Films, *Mater. Res. Innovations*, 2007, **11**(4), 173–176, DOI: 10.1179/143307507X246585.

44 G. K. Hodgson, S. Impellizzeri, G. L. Hallett-Tapley and J. C. Scaiano, Photochemical Synthesis and Characterization of Novel Samarium Oxide Nanoparticles: Toward a Heterogeneous Brønsted Acid Catalyst, *RSC Adv.*, 2015, **5**(5), 3728–3732, DOI: 10.1039/c4ra14841j.

45 B. Fu, T. Jiang and Y. Zhu, Structural Effect of One-Dimensional Samarium Oxide Catalysts on Oxidative Coupling of Methane, *J. Nanosci. Nanotechnol.*, 2017, **18**(5), 3398–3404, DOI: 10.1166/jnn.2018.14647.

46 L. Jiang, Y. Wu, Y. Wang, Q. Zhou, Y. Zheng, Y. Chen and Q. Zhang, A Highly Sensitive and Selective Isobutyraldehyde Sensor Based on Nanosized Sm2O3 Particles, *J. Anal. Methods Chem.*, 2020, **2020**, 5205724, DOI: 10.1155/2020/5205724.

47 M. A. Mora-Ramírez, H. J. Santisteban, M. C. Portillo, A. C. Santiago, A. R. Díaz, V. C. Téllez and O. P. Moreno, Optical Emission Bands of Sm2O3 and Their Link with Crystalline Defects and 4fd→4fd Electronic Transitions at UV-Vis Region, *Optik*, 2021, **241**, 167211, DOI: 10.1016/j.ijleo.2021.167211.

48 R. J. B. Leote, E. Matei, N. G. Apostol, M. Enculescu, I. Enculescu and V. C. Diculescu, Monodispersed Nanoplatelets of Samarium Oxides for Biosensing Applications in Biological Fluids, *Electrochim. Acta*, 2022, **402**, 139532, DOI: 10.1016/j.electacta.2021.139532.

49 M. A. Ruiz-Gómez, C. Gómez-Solís, M. E. Zarazúa-Morín, L. M. Torres-Martínez, I. Juárez-Ramírez, D. Sánchez-Martínez and M. Z. Figueroa-Torres, Innovative Solvo-Combustion Route for the Rapid Synthesis of MoO 3 and Sm2O3 Materials, *Ceram. Int.*, 2014, **40**(1 PART B), 1893–1899, DOI: 10.1016/j.ceramint.2013.07.095.

50 J. Mandal, K. Yoshimura, B. J. Sarkar, A. K. Deb and P. K. Chakrabarti, Introduction of Room Temperature Ferromagnetism in Nanocrystalline Samarium Oxide by Doping of Co-Ion, *J. Electron. Mater.*, 2019, **48**(12), 8047–8053, DOI: 10.1007/s11664-019-07614-8.

51 P. K. Aswathy, N. S. Chitrapriya, K. Sandhya and N. R. Deepthi, Structural Transformation on Transition Metal Doped Sm 2 O 3 Nanomaterials, *Mater. Today: Proc.*, 2019, **10**, 159–165, DOI: 10.1016/j.matpr.2019.02.201.

52 J. Zhang, S. Paydar, N. Akbar and C. Yan, Electrical Properties of Ni-Doped Sm2O3 Electrolyte, *Int. J. Hydrogen Energy*, 2021, **46**(15), 9758–9766, DOI: 10.1016/j.ijhydene.2020.08.057.

53 X. Zhang, L. Liu, J. Feng, X. Ju, J. Wang, T. He and P. Chen, Metal-Support Interaction-Modulated Catalytic Activity of Ru Nanoparticles on Sm2O3for Efficient Ammonia Decomposition, *Catal. Sci. Technol.*, 2021, **11**(8), 2915–2923, DOI: 10.1039/d1cy00080b.

54 S. Ahmadnia-Feyzabad, Y. Mortazavi, A. A. Khodadadi and S. Hemmati, Sm2O3 Doped-SnO2 Nanoparticles, Very Selective and Sensitive to Volatile Organic Compounds, *Sens. Actuators, B*, 2013, **181**, 910–918, DOI: 10.1016/j.snb.2013.02.101.

55 S. Habibzadeh, A. A. Khodadadi and Y. Mortazavi, CO and Ethanol Dual Selective Sensor of Sm2O3-Doped SnO2 Nanoparticles Synthesized by Microwave-Induced Combustion, *Sens. Actuators, B*, 2010, **144**(1), 131–138, DOI: 10.1016/j.snb.2009.10.047.

56 F. I. Shaikh, L. P. Chikhale, J. Y. Patil, I. S. Mulla and S. S. Suryavanshi, Enhanced Acetone Sensing Performance of Nanostructured Sm2O3 Doped SnO2 Thick Films, *J. Rare Earths*, 2017, **35**(8), 813–823, DOI: 10.1016/S1002-0721(17)60981-5.

57 B. Mandal and A. Mondal, Solar Light Sensitive Samarium-Doped Ceria Photocatalysts: Microwave Synthesis, Characterization and Photodegradation of Acid Orange 7 at Atmospheric Conditions and in the Absence of Any Oxidizing Agents, *RSC Adv.*, 2015, **5**(54), 43081–43091, DOI: 10.1039/c5ra03758a.

58 H. C. Yao, X. L. Zhao, X. Chen, J. C. Wang, Q. Q. Ge, J. S. Wang and Z. J. Li, Processing and Characterization of CoO and Sm 2O 3 Codoped Ceria Solid Solution Electrolyte,

J.Power Sources, 2012, **205**, 180–187, DOI: 10.1016/j.jpowsour.2012.01.076.

59 A. A. Ibrahim, A. Umar, R. Kumar, S. H. Kim, A. Bumajdad and S. Baskoutas, Sm2O3-Doped ZnO Beech Fern Hierarchical Structures for Nitroaniline Chemical Sensor, *Ceram. Int.*, 2016, **42**(15), 16505–16511, DOI: 10.1016/j.ceramint.2016.07.061.

60 B. V. Ayodele, M. R. Khan and C. K. Cheng, Greenhouse Gases Abatement by Catalytic Dry Reforming of Methane to Syngas over Samarium Oxide-Supported Cobalt Catalyst, *Int. J. Environ. Sci. Technol.*, 2017, **14**(12), 2769–2782, DOI: 10.1007/s13762-017-1359-2.

61 D. Duan, C. Hao, L. Wang, M. Adil, W. Shi, H. Wang, L. Gao, X. Song and Z. Sun, Novel Nanorod Au/Sm2O3 Catalyst Synthesized by Dealloying Combined with Calcination for Low-Temperature CO Oxidation, *J. Alloys Compd.*, 2020, **818**, 152879, DOI: 10.1016/j.jallcom.2019.152879.

62 Y. Zhu, T. Hai, X. Ji, X. Chen, S. Cui, J. Zhu, X. Xu, J. Zhao and W. Xu, Highly Effective Upconversion Broad-Band Luminescence and Enhancement in Dy2O3/Au and Sm2O3/Au Composites, *J. Lumin.*, 2017, **181**, 352–359, DOI: 10.1016/j.jlumin.2016.09.037.

63 Y. Yu, S. Xu, Y. Gao, M. Jiang, X. Li, J. Zhang, X. Zhang and B. Chen, Enhanced Photothermal Conversion Performances with Ultra-Broad Plasmon Absorption of Au in Au/Sm2O3 Composites, *J. Am. Ceram. Soc.*, 2020, **103**(8), 4420–4428, DOI: 10.1111/jace.17133.

64 M. A. Barakat, AgSm2O3 Nanocomposite for Environmental Remediation of Cyanide from Aqueous Solution, *J. Taiwan Inst. Chem. Eng.*, 2016, **65**, 134–139, DOI: 10.1016/j.jtice.2016.04.020.

65 W. Zhang, C. Lu, Y. Ni, J. Song and Z. Xu, Preparation and Characterization of Sm 2O 3/Cu Mosaic Structure with Infrared Absorptive Properties and Low Infrared Emissivity, *Mater. Lett.*, 2012, **87**, 13–16, DOI: 10.1016/j.matlet.2012.07.044.

66 X. Y. Zhu, J. Zhang, L. M. Luo, J. Chen, J. G. Cheng and Y. C. Wu, Microstructure and Properties of W/Sm2O3 Composites Prepared Spark Plasma Sintering, *Adv. Powder Technol.*, 2015, **26**(2), 640–643, DOI: 10.1016/j.apt.2015.01.015.

67 X. Y. Ding, L. M. Luo, X. Y. Tan, G. N. Luo, P. Li, X. Zan, J. G. Cheng and Y. C. Wu, Microstructure and Properties of Tungsten-Samarium Oxide Composite Prepared by a Novel Wet Chemical Method and Spark Plasma Sintering, *Fusion Eng. Des.*, 2014, **89**(6), 787–792, DOI: 10.1016/j.fusengdes.2014.05.025.

68 N. Ullah, Z. Song, W. Liu, C. C. Kuo, A. Ramiere and X. Cai, Photo-Promoted in Situ Reduction and Stabilization of Pd Nanoparticles by H2 at Photo-Insensitive Sm2O3 Nanorods, *J. Colloid Interface Sci.*, 2022, **607**, 479–487, DOI: 10.1016/j.jcis.2021.08.184.

69 T. W. Chen, U. Rajaji, S. M. Chen, R. J. Ramalingam and X. Liu, Developing Green Sonochemical Approaches towards the Synthesis of Highly Integrated and Interconnected Carbon Nanofiber Decorated with Sm2O3 Nanoparticles and Their Use in the Electrochemical Detection of Toxic 4-Nitrophenol, *Ultrason. Sonochem.*, 2019, **58**(April), 104595, DOI: 10.1016/j.ultsonch.2019.05.012.

70 J. He, F. Qiu, Q. Xu, J. An and R. Qiu, A Carbon Nanofibers-Sm2O3 Nanocomposite: A Novel Electrochemical Platform for Simultaneously Detecting Two Isomers of Dihydroxybenzene, *Anal. Methods*, 2018, **10**(16), 1852–1862, DOI: 10.1039/c7ay02981k.

71 J. Ilsemann, A. Sonström, T. M. Gesing, R. Anwander and M. Bäumer, Highly Active Sm 2 O 3 -Ni Xerogel Catalysts for CO 2 Methanation, *ChemCatChem*, 2019, **11**(6), 1732–1741, DOI: 10.1002/cctc.201802049.

72 S. R. Jamnani, H. M. Moghaddam, S. G. Leonardi and G. Neri, PANI/Sm2O3 Nanocomposite Sensor for Fast Hydrogen Detection at Room Temperature, *Synth. Met.*, 2020, **268**(May), 116493, DOI: 10.1016/j.synthmet.2020.116493.

73 Y. Liu, K. Wang, Z. Huang, X. Zheng and J. Wen, Enhanced Photo-Fenton Activity of Sm2O3–NiO Heterojunction under Visible Light Irradiation, *J. Alloys Compd.*, 2019, **800**, 498–504, DOI: 10.1016/j.jallcom.2019.06.129.

74 F. Mesgari, S. M. Beigi, F. Salehnia, M. Hosseini and M. R. Ganjali, Enhanced Electrochemiluminescence of Ru(Bpy)32+ by Sm2O3 Nanoparticles Decorated Graphitic Carbon Nitride Nano-Sheets for Pyridoxine Analysis, *Inorg. Chem. Commun.*, 2019, **106**(April), 240–247, DOI: 10.1016/j.inoche.2019.05.023.

75 S. Biswas, H. Naskar, S. Pradhan, Y. Chen, Y. Wang, R. Bandyopadhyay and P. Pramanik, Sm2O3 Nanorod-Modified Graphite Paste Electrode for Trace Level Voltammetric Determination of Acetaminophen and Ciprofloxacin, *New J. Chem.*, 2020, **44**(5), 1921–1930, DOI: 10.1039/c9nj04446a.

76 I. Muneer, M. A. Farrukh, S. Javaid, M. Shahid and M. Khaleeq-Ur-Rahman, Synthesis of Gd2O3/Sm2O3 Nanocomposite via Sonication and Hydrothermal Methods and Its Optical Properties, *Superlattices Microstruct.*, 2015, **77**, 256–266, DOI: 10.1016/j.spmi.2014.10.006.

77 J. Zeng, Z. Li, H. Peng and X. Zheng, Core-Shell Sm2O3@ZnO Nano-Heterostructure for the Visible Light Driven Photocatalytic Performance, *Colloids Surf., A*, 2019, **560**(October 2018), 244–251, DOI: 10.1016/j.colsurfa.2018.10.023.

78 M. Bagheri, N. F. Hamedani, A. R. Mahjoub, A. A. Khodadadi and Y. Mortazavi, Highly Sensitive and Selective Ethanol Sensor Based on Sm2O 3-Loaded Flower-like ZnO Nanostructure, *Sens. Actuators, B*, 2014, **191**, 283–290, DOI: 10.1016/j.snb.2013.10.001.

79 X. Zhang, M. He, P. He, H. Liu, H. Bai, J. Chen, S. He, X. Zhang, F. Dong and Y. Chen, Hierarchical Structured Sm 2 O 3 Modified CuO Nanoflowers as Electrode Materials for High Performance Supercapacitors, *Appl. Surf. Sci.*, 2017, **426**, 933–943, DOI: 10.1016/j.apsusc.2017.07.236.

80 Y. Zhang, P. He, L. Jia, C. Li, H. Liu, S. Wang, S. Zhou and F. Dong, Ti/PbO2-Sm2O3 Composite Based Electrode for

Highly Efficient Electrocatalytic Degradation of Alizarin Yellow R, *J. Colloid Interface Sci.*, 2019, **533**, 750–761, DOI: 10.1016/j.jcis.2018.09.003.

81 A. S. Dezfuli, M. R. Ganjali and H. R. Naderi, Anchoring Samarium Oxide Nanoparticles on Reduced Graphene Oxide for High-Performance Supercapacitor, *Appl. Surf. Sci.*, 2017, **402**, 245–253, DOI: 10.1016/j.apsusc.2017.01.021.

82 M. Sai Bhargava Reddy, B. Geeta Rani, S. Kailasa, N. Jayarambabu, P. Munindra, N. Kundana and K. Venkateswara Rao, Sm2O3 Rice-like Nanorods Decorated on RGO Flexible Resistive Sensor for Room Temperature LPG Detection, *Mater. Sci. Eng. B: Solid-State Mater. Adv. Technol.*, 2020, **262**(May), 114757, DOI: 10.1016/j.mseb.2020.114757.

83 T. Sakthi Priya, N. Nataraj, T. W. Chen, S. M. Chen and T. Kokulnathan, Synergistic Formation of Samarium Oxide/Graphene Nanocomposite: A Functional Electrocatalyst for Carbendazim Detection, *Chemosphere*, 2022, **307**(Part 1), 135711, DOI: 10.1016/j.chemosphere.2022.135711.

84 Y. Li, D. He, Z. Zhu, Q. Zhu and B. Xu, Properties of Sm2O3-ZrO2 Composite Oxides and Their Catalytic Performance in Isosynthesis, *Appl. Catal., A*, 2007, **319**, 119–127, DOI: 10.1016/j.apcata.2006.11.020.

85 R. Liu, L. S. Qiang, W. D. Yang and H. Y. Liu, Enhanced Conversion Efficiency of Dye-Sensitized Solar Cells Using Sm 2O 3-Modified TiO 2 Nanotubes, *J. Power Sources*, 2013, **223**, 254–258, DOI: 10.1016/j.jpowsour.2012.09.045.

86 L. M. Gómez-Sainero, R. T. Baker, I. S. Metcalfe, M. Sahibzada, P. Concepción and J. M. López-Nieto, Investigation of Sm2O3-CeO2-Supported Palladium Catalysts for the Reforming of Methanol: The Role of the Support, *Appl. Catal., A*, 2005, **294**(2), 177–187, DOI: 10.1016/j.apcata.2005.07.022.

87 R. T. Baker, L. M. Gómez-Sainero and I. S. Metcalfe, Pretreatment-Induced Nanostructural Evolution in CeO2-, Sm 2O3-, and CeO2/ Sm2O 3-Supported Pd Catalysts for Intermediate-Temperature Methanol Fuel Cells, *J. Phys. Chem. C*, 2009, **113**(28), 12465–12475, DOI: 10.1021/jp8075194.

88 X. Zheng, F. Kang, C. Huang, S. Lv, J. Zhang and H. Peng, Enhanced Photocatalytic Capacity of ZnS–ZnO–Sm2O3 Composites for the Removal of Dyes and Antibiotics in Visible Light Region, *J. Ind. Eng. Chem.*, 2020, **88**(2019), 186–195, DOI: 10.1016/j.jiec.2020.04.012.

89 Q. Liu, H. Yang, H. Dong, W. Zhang, B. Bian, Q. He, J. Yang, X. Meng, Z. Tian and G. Zhao, Effects of Preparation Method and Sm2O3 Promoter on CO Methanation by a Mesoporous NiO-Sm2O3/Al2O3 Catalyst, *New J. Chem.*, 2018, **42**(15), 13096–13106, DOI: 10.1039/c8nj02282h.

90 B. Han, N. Chen, D. Deng, S. Deng, I. Djerdj and Y. Wang, Enhancing Phosphate Removal from Water by Using Ordered Mesoporous Silica Loaded with Samarium Oxide, *Anal. Methods*, 2015, **7**(23), 10052–10060, DOI: 10.1039/c5ay02319j.

91 N. A. Ayub, H. Bahruji and A. H. Mahadi, Barium Promoted Ni/Sm 2 O 3 Catalysts for Enhanced CO 2 Methanation, *RSC Adv.*, 2021, **11**(50), 31807–31816, DOI: 10.1039/d1ra04115k.

92 T. W. Chen, U. Rajaji, S. M. Chen, R. J. Ramalingam and X. Liu, Developing Green Sonochemical Approaches towards the Synthesis of Highly Integrated and Interconnected Carbon Nanofiber Decorated with Sm2O3 Nanoparticles and Their Use in the Electrochemical Detection of Toxic 4-Nitrophenol, *Ultrason. Sonochem.*, 2019, **58**(April), 104595, DOI: 10.1016/j.ultsonch.2019.05.012.

93 R. Florez, H. A. Colorado, C. H. C. Giraldo and A. Alajo, Preparation and Characterization of Portland Cement Pastes with Sm2O3 Microparticle Additions for Neutron Shielding Applications, *Constr. Build. Mater.*, 2018, **191**, 498–506, DOI: 10.1016/j.conbuildmat.2018.10.019.

94 S. Y. Huang, T. C. Chang, M. C. Chen, S. C. Chen, H. P. Lo, H. C. Huang, D. S. Gan, S. M. Sze and M. J. Tsai, Resistive Switching Characteristics of Sm2O3 Thin Films for Nonvolatile Memory Applications, *Solid-State Electron.*, 2011, **63**(1), 189–191, DOI: 10.1016/j.sse.2011.04.012.

95 N. F. Zulkipli, M. Batumalay, F. S. M. Samsamnun, M. B. H. Mahyuddin, T. F. T. M. N. Izam, M. I. M. A. Khudus and S. W. Harun, Q-Switching Pulses Generation with Samarium Oxide Film Saturable Absorber, *Microw. Opt. Technol. Lett.*, 2020, **62**(3), 1049–1055, DOI: 10.1002/mop.32118.

96 J. Yoshikawa, Y. Katsuda, N. Yamada, C. Ihara, M. Masuda and H. Sakai, Effects of Samarium Oxide Addition on the Phase Composition, Microstructure, and Electrical Resistivity of Aluminum Nitride Ceramics, *J. Am. Ceram. Soc.*, 2005, **88**(12), 3501–3506, DOI: 10.1111/j.1551-2916.2005.00637.x.

97 M. Jourshabani, Z. Shariatinia and A. Badiei, Synthesis and Characterization of Novel Sm 2 O 3 /S-Doped g-C 3 N 4 Nanocomposites with Enhanced Photocatalytic Activities under Visible Light Irradiation, *Appl. Surf. Sci.*, 2018, **427**, 375–387, DOI: 10.1016/j.apsusc.2017.08.051.

98 O. P. Moreno, R. G. Pérez, R. P. Merino, M. C. Portillo, M. N. M. Specia, M. H. Hernández, S. S. Sauceda and E. R. Rosas, Growth of Sm(OH)3 Nanocrystals by Chemical Bath Deposition and Its Thermal Annealing Treatment to Sm2O3, *Optik*, 2017, **135**, 70–78, DOI: 10.1016/j.ijleo.2017.01.077.

99 M. A. M. Khan, W. Khan, M. Ahamed and A. N. Alhazaa, Microstructural Properties and Enhanced Photocatalytic Performance of Zn Doped CeO2 Nanocrystals, *Sci. Rep.*, 2017, **7**(1), 1–11, DOI: 10.1038/s41598-017-11074-7.

100 X. Zheng, K. Wang, Z. Huang, Y. Liu, J. Wen and H. Peng, MgO Nanosheets with N-Doped Carbon Coating for the Efficient Visible-Light Photocatalysis, *J. Ind. Eng. Chem.*, 2019, **76**, 288–295, DOI: 10.1016/j.jiec.2019.03.053.

101 L. Yu, W. Chen, D. Li, J. Wang, Y. Shao, M. He, P. Wang and X. Zheng, Inhibition of Photocorrosion and Photoactivity Enhancement for ZnO via Specific Hollow ZnO Core/ZnS Shell Structure, *Appl. Catal., B*, 2015, **164**, 453–461, DOI: 10.1016/j.apcatb.2014.09.055.

102 Y. Liu, K. Wang, Z. Huang, X. Zheng and J. Wen, Enhanced Photo-Fenton Activity of Sm2O3–NiO Heterojunction under Visible Light Irradiation, *J. Alloys Compd.*, 2019, **800**, 498–504, DOI: 10.1016/j.jallcom.2019.06.129.

103 Y. Liu, S. Shen, J. Zhang, W. Zhong and X. Huang, Cu2−xSe/CdS Composite Photocatalyst with Enhanced Visible Light Photocatalysis Activity, *Appl. Surf. Sci.*, 2019, **478**, 762–769, DOI: 10.1016/j.apsusc.2019.02.010.

104 X. Zheng, Y. Hu, Z. Li, Y. Dong, J. Zhang, J. Wen and H. Peng, Sm 2 O 3 Nanoparticles Coated with N-Doped Carbon for Enhanced Visible-Light Photocatalysis, *J. Phys. Chem. Solids*, 2019, **130**(February), 180–188, DOI: 10.1016/j.jpcs.2019.02.032.

105 T. Teker and M. Aslanoglu, Sensitive and Selective Determination of Paracetamol Using a Composite of Carbon Nanotubes and Nanoparticles of Samarium Oxide and Zirconium Oxide, *Microchem. J.*, 2020, **158**(April), 105234, DOI: 10.1016/j.microc.2020.105234.

106 C. Constantinescu, V. Ion, A. C. Galca and M. Dinescu, Morphological, Optical and Electrical Properties of Samarium Oxide Thin Films, *Thin Solid Films*, 2012, **520**(20), 6393–6397, DOI: 10.1016/j.tsf.2012.06.049.

107 H. Liu, S. Zeng, P. He, F. Dong, M. He, Y. Zhang, S. Wang, C. Li, M. Liu and L. Jia, Samarium Oxide Modified Ni-Co Nanosheets Based Three-Dimensional Honeycomb Film on Nickel Foam: A Highly Efficient Electrocatalyst for Hydrogen Evolution Reaction, *Electrochim. Acta*, 2019, **299**, 405–414, DOI: 10.1016/j.electacta.2018.12.169.

108 M. Hosseini, M. R. Moghaddam, F. Faridbod, P. Norouzi, M. R. K. Pur and M. R. Ganjali, A Novel Solid-State Electrochemiluminescence Sensor Based on a Ru(Bpy)32+/Nano Sm2O3 Modified Carbon Paste Electrode for the Determination of L-Proline, *RSC Adv.*, 2015, **5**(79), 64669–64674, DOI: 10.1039/c5ra06897e.

109 Q. Zhou, C. Tang, S. P. Zhu, W. G. Chen and J. Li, Synthesis, Characterisation and Sensing Properties of Sm2O3 Doped SnO2 Nanorods to C2H2 Gas Extracted from Power Transformer Oil, *Mater. Technol.*, 2016, **31**(6), 364–370, DOI: 10.1179/1753555715Y.0000000069.

110 A. S. Jones, D. Aziz, J. Ilsemann, M. Bäumer and H. Hagelin-Weaver, Doped Samarium Oxide Xerogels for Oxidative Coupling of Methane—Effects of High-Valence Dopants at Very Low Concentrations, *Catal. Today*, 2021, **365**(February), 46–57, DOI: 10.1016/j.cattod.2020.06.012.

111 S. R. Jamnani, H. M. Moghaddam, S. G. Leonardi and G. Neri, A Novel Conductometric Sensor Based on Hierarchical Self-Assembly Nanoparticles Sm2O3 for VOCs Monitoring, *Ceram. Int.*, 2018, **44**(14), 16953–16959, DOI: 10.1016/j.ceramint.2018.06.136.

112 Q. Zhou, M. Cao, W. Li, C. Tang and S. Zhu, Research on Acetylene Sensing Properties and Mechanism of SnO2 Based Chemical Gas Sensor Decorated with Sm2O3, *J. Nanotechnol.*, 2015, **2015**, 714072, DOI: 10.1155/2015/714072.

113 K. Velsankar, S. Sudhahar, G. Parvathy and R. Kaliammal, Effect of Cytotoxicity and AAntibacterial Activity of Biosynthesis of ZnO Hexagonal Shaped Nanoparticles by Echinochloa Frumentacea Grains Extract as a Reducing Agent, *Mater. Chem. Phys.*, 2020, **239**, 121976, DOI: 10.1016/j.matchemphys.2019.121976.

114 K. Ramanujam and M. Sundrarajan, Antibacterial Effects of Biosynthesized MgO Nanoparticles Using Ethanolic Fruit Extract of Emblica Officinalis, *J. Photochem. Photobiol., B*, 2014, **141**, 296–300, DOI: 10.1016/j.jphotobiol.2014.09.011.

115 S. Kokilavani, A. Syed, M. Raaja Rajeshwari, V. Subhiksha, A. M. Elgorban, A. H. Bahkali, N. S. S. Zaghloul, A. Das and S. Sudheer Khan, Decoration of Ag2WO4 on Plate-like MnS for Mitigating the Charge Recombination and Tuned Bandgap for Enhanced White Light Photocatalysis and Antibacterial Applications, *J. Alloys Compd.*, 2021, **889**, 161662, DOI: 10.1016/j.jallcom.2021.161662.

116 G. Sharmila, M. Thirumarimurugan and C. Muthukumaran, Green Synthesis of ZnO Nanoparticles Using Tecoma Castanifolia Leaf Extract: Characterization and Evaluation of Its Antioxidant, Bactericidal and Anticancer Activities, *Microchem. J.*, 2019, **145**, 578–587, DOI: 10.1016/j.microc.2018.11.022.

117 M. Khatami, H. Q. Alijani, B. Fakheri, M. M. Mobasseri, M. Heydarpour, Z. K. Farahani and A. U. Khan, Super-Paramagnetic Iron Oxide Nanoparticles (SPIONs): Greener Synthesis Using Stevia Plant and Evaluation of Its Antioxidant Properties, *J. Cleaner Prod.*, 2019, **208**, 1171–1177, DOI: 10.1016/j.jclepro.2018.10.182.

